

Chaotic Dynamics of the Mass Deformed ABJM Model

K. Başkan^a, S. Kürkçüoğlu^a, C. Taşcı^{a,b}

^a *Middle East Technical University, Department of Physics,
Dumlupınar Boulevard, 06800, Ankara, Turkey*

^b *The Graduate Center, City University of New York
365 Fifth Ave, New York, NY 10016, U.S.A.*

E-mails: kagan.baskan@metu.edu.tr
kseckin@metu.edu.tr
ctasci@gradcenter.cuny.edu

Abstract

We explore the chaotic dynamics of the mass deformed ABJM model. To do so, we first perform a dimensional reduction of this model from $2 + 1$ - to $0 + 1$ -dimensions, considering that the fields are spatially uniform. Working in the 't Hooft limit and tracing over ansatz configurations involving fuzzy two-spheres, which are described in terms of the GRVV matrices with collective time dependence, we obtain a family of reduced effective Lagrangians and demonstrate that they have chaotic dynamics by computing the associated Lyapunov exponents. In particular, we focus on how the largest Lyapunov exponent, λ_L , changes as a function of E/N^2 . Depending on the structure of the effective potentials, we find either $\lambda_L \propto (E/N^2)^{1/3}$ or $\lambda_L \propto (E/N^2 - \gamma_N)^{1/3}$, where $\gamma_N(k, \mu)$ is a constant determined in terms of the Chern-Simons coupling k , the mass μ , and the matrix level N . Using our results, we investigate the temperature dependence of the largest Lyapunov exponents and give upper bounds on the temperature above which λ_L values comply with the MSS bound, $\lambda_L \leq 2\pi T$, and below which it will eventually be violated.

1 Introduction

Studies on exploring the structure of chaotic dynamics emerging from the matrix quantum mechanics have been continuing with growing interest for quite sometime [1–14]. Early investigations on the chaotic dynamics of Yang-Mills (YM) gauge theories dates back to 80's [15–17] and in the context of the Banks-Fischler-Shenker-Susskind (BFSS) model [18] to the work Arefeva et. al. [19]. Recent studies are especially motivated by a result due Maldacena-Shenker-Stanford (MSS) [6], which briefly states that, under rather general conditions met by a physical system, the largest Lyapunov exponent (which is a measure of chaos in both classical and quantum mechanical systems) for quantum chaotic dynamics is controlled by a temperature dependent bound and given by $\lambda_L \leq 2\pi T$. It is conjectured that systems which are holographically dual to the black holes are maximally chaotic, meaning that they saturate this bound. This is already demonstrated for a particular fermionic matrix model, namely the Sachdev-Ye-Kitaev (SYK) [7] model, and expected to be so for other matrix models which have a holographic dual such as the BFSS [18] model. The latter and the Berenstein-Maldacena-Nastase (BMN) model [20] are supersymmetric $SU(N)$ gauge theories, describing the dynamics of the N -coincident $D0$ -branes in the flat and spherical backgrounds, respectively and also appear in the DLCQ quantization of M-theory in the flat and the pp-wave backgrounds [18, 20–25]. It is well-known that the gravity dual of the BFSS model is obtained in the 't Hooft limit and describes a phase in which $D0$ -branes form a so called black-brane, i.e. a string theoretical black hole [24–26].

Classical dynamics of YM matrix models provide a good approximation of the high temperature limit of the quantum theory. Although this regime is distinguished from that in which the gravity dual is obtained (i.e. the low temperature limit), early numerical studies conducted in [27, 28] gave no indication of an occurrence of a phase transition between the low and high temperature limits, which makes it quite plausible that some features like fast scrambling [1] of black holes gravity dual, or temperature dependence of chaotic dynamics may be retained to a certain extent at the high temperature limit too. For instance, the numerical results obtained in [2] by exploiting the classical dynamics of the BMN model results in a fast thermalization. In [4], classical chaotic dynamics of the BFSS models is studied and there it is found that the largest Lyapunov exponent is given as $\lambda_L = 0.2924(3)(\lambda_{t\text{Hooft}} T)^{1/4}$. Therefore, the MSS bound is violated only at temperatures below the critical temperature $T_c \approx 0.015$ while it remains parametrically smaller than $2\pi T$ for $T > T_c$. In [14], we have studied chaos in massive deformations of the $SU(N)$ Yang-Mills gauge theories in $0 + 1$ -dimensions, with the same matrix content as that of the bosonic part of the BFSS model, by making use of ansatz configurations involving both fuzzy two- and four-spheres. Our numerical results have shown very good agreement with the $\lambda_L \propto (E/N^2)^{1/4}$ type functional behaviour of the largest Lyapunov exponent with energy, which, together with the application of the virial and the equipartition theorems, allowed us to put upper bounds on the critical temperature, T_c . Depending on the values of the mass parameters, our estimates for T_c were around twice or about an order of magnitude

larger than that obtained for the BFSS model in [4]. In the present paper, we extend and apply the methods we have developed in [14] to another interesting gauge theory, namely the massive deformation of the Aharony-Bergman-Jafferis-Maldacena (ABJM) model [29]. Before focusing our attention in this direction, let us also note that not only the BFSS and the BMN matrix models, but even their subsectors at small values of N are quite non-trivial many-body systems, which escape a complete solution to this day. Nevertheless, the chaotic dynamics of the smallest YM matrix model composed of two 2×2 Hermitian matrices with $SU(2)$ gauge and $SO(2)$ global symmetries is recently explored in [5] (see also the references [30, 31] in this context) with the chaotic phase, corresponding to a toy model for a black hole, being controlled by the angular momentum associated to the rigid $SO(2)$ symmetry. In [32], two of us explored the minimal Yang-Mills-Chern-Simons matrix model and analyzed the effect of the Chern-Simons (CS) coupling on the chaotic dynamics.

As is well-known, ABJM model is a $2 + 1$ dimensional $\mathcal{N} = 6$ supersymmetric $SU(N) \times SU(N)$ Chern-Simons (CS) gauge theory at the CS level $(-k, k)$ [29] and describes the dynamics of N coincident $M2$ -branes [29, 33]. This model consists of four complex scalar fields C^I ($I : 1, 2, 3, 4$), as would be expected due to the eight transverse directions to the $M2$ -branes, and four Majorana fermions ψ^I to match the bosonic and fermionic degrees of freedom as a minimal requirement for the presence of supersymmetry. These fields are coupled bifundamentally to the $SU(N)$ CS gauge fields A_μ and \hat{A}_μ , i.e. they carry the (N, \bar{N}) representation of the $SU(N) \times SU(N)$ group. The model has the R -symmetry group $U(1) \times SU(4)$ under which both the complex scalars and the fermions transform in the 4-dimensional fundamental representation of $SU(4)$ and carry $+1$ charge under the $U(1)$ factor. ABJM model is dual to type IIA string theory on $AdS_4 \times S^7/\mathbb{Z}^k$ (this becomes $AdS_4 \times \mathbb{C}P^3$ in the $k \rightarrow \infty$ limit) via the AdS/CFT correspondence [29, 33] and it possess a massive deformation preserving all the supersymmetry, but breaking the R -symmetry. It is this model that we focus our attention in the present paper. The vacuum configurations in this model are given by the so called Rodriguez-Gomez, Van Raamsdonk and Verlinde (GRVV) matrices [35], which describe fuzzy two-spheres as a somewhat intricate analysis demonstrates [33]. This feature is similar and comparable to the BMN model, which also has fuzzy spheres as the vacuum solutions. Our aim here is to explore the chaotic dynamics emerging from this model at the classical level using both analytic and numeric techniques and determine upper bounds on the temperature of the system at consecutively higher matrix levels, above which the MSS bound is satisfied and below which it will eventually be violated. The latter is naturally expected to occur, since, as we already noted, the classical treatment of the model could approximate the dynamics of the full quantum theory only at sufficiently high temperatures. Toward this aim, we first perform a dimensional reduction of this model from $2 + 1$ - to $0 + 1$ -dimensions by considering that the fields are spatially uniform. We work in the 't Hooft limit and focus on two distinct ansatz configurations both involving fuzzy two-spheres, which are described in terms of the GRVV matrices. These configurations have collective time-dependence, which are introduced by real functions of time multiplying the

latter. Tracing over these configurations yields a family of reduced effective Lagrangians and we demonstrate that they have chaotic dynamics by computing their Lyapunov exponents. In particular, we direct our attention to examine how the largest Lyapunov exponent, λ_L , changes as a function of E/N^2 . It turns out that, depending on the structure of the effective potentials, we find either that $\lambda_L \propto (E/N^2)^{1/3}$ or $\lambda_L \propto (E/N^2 - \gamma_N)^{1/3}$, where $\gamma_N(k, \mu)$ is a constant determined in terms of the CS coupling k , the mass μ , and the matrix level N . This power law response of λ_L to energy is also anticipated and supported by the exact scaling symmetry possessed by the model in the massless limit as will be discussed in the next section. Making use of our numerical results, and evoking the virial and equipartition theorems, we explore the implications for the aforementioned MSS conjecture in the context of this model. The main outcomes are the upper bounds we obtain on the temperatures above which largest Lyapunov exponents comply with the MSS bound and below which it will eventually be violated. At the same time, we demonstrate that with increasing matrix level, i.e. with better numerical approximation of the 't Hooft limit, estimates of T_c display a decreasing trend, put it differently, the temperature range in which the MSS bound is valid expands gradually.

The paper is organized as follows. In section 2, we outline and review the various features of the massive deformation of the ABJM model and obtain its reduction from $2 + 1$ - to $0 + 1$ -dimensions by assuming spatially uniform fields. In section 3, we introduce our first ansatz configuration, obtain the reduced effective actions, and present the results of the numerical analysis leading to the modeling of the energy dependence of the largest Lyapunov exponent. This is followed by the discussion explaining how we extract the temperature dependence and relate our findings to the MSS conjecture. In section 4, results of an analysis following mainly the same steps of section 3 are presented for another ansatz configuration. Several details of the calculations are relegated to the appendices A and B. We conclude in section 5 by briefly summarizing our results and indicating some directions for future studies.

2 Reduction of Mass Deformed ABJM Mode to $0 + 1$ -Dimensions

We start with writing out the action for the bosonic part of the mass deformed ABJM model. This is given as [35]

$$S_{ABJM} = \int d^3x \frac{k}{4\pi} \epsilon^{\mu\nu\lambda} \text{Tr} \left(A_\mu \partial_\nu A_\lambda + \frac{2i}{3} A_\mu A_\nu A_\lambda - \hat{A}_\mu \partial_\nu \hat{A}_\lambda - \frac{2i}{3} \hat{A}_\mu \hat{A}_\nu \hat{A}_\lambda \right) - \text{Tr} |D_\mu Q^\alpha|^2 - \text{Tr} |D_\mu R^\alpha|^2 - V, \quad (2.1)$$

where A_μ and \hat{A}_μ ($\mu : 0, 1, 2$) are two distinct gauge fields transforming under the $SU(N)_k$ and $SU(N)_{-k}$ gauge transformations, respectively. The subscripts $\pm k \in \mathbb{Z}$ label the level of the Chern-Simons terms associated to these gauge fields. The potential term is given as

$$V = \text{Tr} \left(|M^\alpha|^2 + |N^\alpha|^2 \right), \quad (2.2)$$

where

$$\begin{aligned} M^\alpha &= \mu Q^\alpha + \frac{2\pi}{k} (2Q^{[\alpha} Q_\beta^\dagger Q^{\beta]} + R^\beta R_\beta^\dagger Q^\alpha - Q^\alpha R_\beta^\dagger R^\beta + 2Q^\beta R_\beta^\dagger R^\alpha - 2R^\alpha R_\beta^\dagger Q^\beta), \\ N^\alpha &= -\mu R^\alpha + \frac{2\pi}{k} (2R^{[\alpha} R_\beta^\dagger R^{\beta]} + Q^\beta Q_\beta^\dagger R^\alpha - R^\alpha Q_\beta^\dagger Q^\beta + 2R^\beta Q_\beta^\dagger Q^\alpha - 2Q^\alpha Q_\beta^\dagger R^\beta). \end{aligned} \quad (2.3)$$

In this expression $(Q^\alpha, R^\alpha) := C^I$ with $(\alpha : 1, 2)$ and $(I : 1, 2, 3, 4)$ are complex bi-fundamental scalar fields, i.e. they transform as $Q^\alpha \rightarrow U_L Q^\alpha U_R$, $R^\alpha \rightarrow U_L R^\alpha U_R$, where $(U_L, U_R) \in SU(N)_k \times SU(N)_{-k}$. The covariant derivatives are given as

$$\begin{aligned} D_\mu Q^\alpha &= \partial_\mu Q^\alpha + iA_\mu Q^\alpha - iQ^\alpha \hat{A}_\mu, \\ D_\mu R^\alpha &= \partial_\mu R^\alpha + iA_\mu R^\alpha - iR^\alpha \hat{A}_\mu, \end{aligned} \quad (2.4)$$

and μ stands for the mass of the fields (Q^α, R^α) . $e^{iS_{ABJM}}$ is invariant under the gauge group $SU(N)_k \times SU(N)_{-k}$ provided that $k \in \mathbb{Z}$. The latter is the level quantization of the Chern Simons couplings in the action. In (2.3), we use the notation

$$Q^{[\alpha} Q_\beta^\dagger Q^{\beta]} = Q^\alpha Q_\beta^\dagger Q^\beta - Q^\beta Q_\beta^\dagger Q^\alpha, \quad (2.5)$$

and likewise for R^{α} 's.

ABJM model has the global $SU(4)_R \times U(1)_R$ R-symmetry group, which is broken down to $SU(2) \times SU(2) \times U(1)_A \times U(1)_B \times \mathbb{Z}_2$ by the mass deformation terms given in M^α and N^α . If there is no mass deformation, it is suitable to formulate the theory in terms of the complex scalar fields C^I , which transform under the 4-dimensional fundamental representation of the $SU(4)_R$ factor and carry $U(1)_R$ charge +1. In the mass deformed model, Q^α transform under the first and R^α under the second of the $SU(2)$ factors of the R-symmetry group, and under $U(1)_A$ they have the charges 1, -1, respectively, while under $U(1)_B$, they both have charge 1, and the \mathbb{Z}_2 factor serves to exchange Q^α and R^α .

In order to dimensionally reduce S_{ABJM} to 0+1-dimensions we declare that all field are independent of the spatial coordinates and depend on time only. Consequently, all partial derivatives with respect to the spatial coordinates vanish. We may introduce the notation $A_\mu \equiv (A_0, X_i)$, $\hat{A}_\mu \equiv (\hat{A}_0, \hat{X}_i)$ with $(i = 1, 2)$. Spatial and time components of the covariant derivative are then

$$\begin{aligned} D_i Q^\alpha &= iX_i Q^\alpha - iQ^\alpha \hat{X}_i, & D_i R^\alpha &= iX_i R^\alpha - iR^\alpha \hat{X}_i, \\ D_0 Q^\alpha &= \partial_0 Q^\alpha + iA_0 Q^\alpha - iQ^\alpha \hat{A}_0, & D_0 R^\alpha &= \partial_0 R^\alpha + iA_0 R^\alpha - iR^\alpha \hat{A}_0, \end{aligned} \quad (2.6)$$

and the action takes the following form,

$$\begin{aligned} S_{ABJM-R} &= N \int dt \frac{k}{4\pi} \text{Tr} \left(-\epsilon^{ij} X_i \dot{X}_j + i\epsilon^{ij} A_0 [X_i, X_j] \right) - \frac{k}{4\pi} \text{Tr} \left(-\epsilon^{ij} \hat{X}_i \dot{\hat{X}}_j + i\epsilon^{ij} \hat{A}_0 [\hat{X}_i, \hat{X}_j] \right) \\ &\quad + \text{Tr} \left(|D_0 Q^\alpha|^2 \right) - \text{Tr} \left(|D_i Q^\alpha|^2 \right) + \text{Tr} \left(|D_0 R^\alpha|^2 \right) - \text{Tr} \left(|D_i R^\alpha|^2 \right) - V. \end{aligned} \quad (2.7)$$

Expressing the Chern-Simons parts of this action in terms of the covariant derivatives $\mathcal{D}_0 X_i := \partial_0 X_i - i[A_0, X_i]$, and $\hat{\mathcal{D}}_0 \hat{X}_i := \partial_0 \hat{X}_i - i[\hat{A}_0, \hat{X}_i]$, we may as well write

$$S_{ABJM-R} = N \int dt - \frac{k}{4\pi} \text{Tr}(\epsilon^{ij} X_i \mathcal{D}_0 X_j) + \frac{k}{4\pi} \text{Tr}(\epsilon^{ij} \hat{X}_i \hat{\mathcal{D}}_0 \hat{X}_j) + \text{Tr}(|D_0 Q^\alpha|^2) - \text{Tr}(|D_i Q^\alpha|^2) + \text{Tr}(|D_0 R^\alpha|^2) - \text{Tr}(|D_i R^\alpha|^2) - V. \quad (2.8)$$

In (2.7) and (2.8) it is understood that all fields depend on time only. We have readily written the reduced action in the 't Hooft limit. The latter is defined as follows. While reducing from $2+1$ to $0+1$ -dimensions, we have integrated over the two-dimensional space whose volume may be denoted, say, by V_2 . Therefore, we may introduce¹ $\lambda'_{tHooft} := \frac{N}{V_2}$ and require that it remains finite in the limit $V_2 \rightarrow \infty$ and $N \rightarrow \infty$. In S_{ABJM-R} , we have scaled λ'_{tHooft} to unity. If needed, it is possible to restore λ'_{tHooft} back in S_{ABJM-R} by performing the scalings $X_i \rightarrow \lambda^{-1/2} X_i$, $\hat{X}_i \rightarrow \lambda^{-1/2} \hat{X}_i$, $A_0 \rightarrow \lambda^{-1/2} A_0$, $\hat{A}_0 \rightarrow \lambda^{-1/2} \hat{A}_0$, $Q_\alpha \rightarrow \lambda^{-1/4} Q_\alpha$, $R_\alpha \rightarrow \lambda^{-1/4} R_\alpha$, $\mu \rightarrow \lambda^{-1/2} \mu$ and $t \rightarrow \lambda^{1/2} t$. Let us note also that S_{ABJM-R} is manifestly gauge invariant under the $SU(N)_k \times SU(N)_{-k}$ gauge symmetry².

The ground states of this reduced model is the same as that of the original model and given by configurations minimizing the potential V in (2.2). Since the latter is positive definite, its minimum is zero and are given by the configurations

$$M^\alpha = 0 = N^\alpha. \quad (2.9)$$

There are two immediate solutions to (2.9), which are given as

$$\begin{aligned} R^\alpha &= c G^\alpha, & Q^\alpha &= 0, \\ R^\alpha &= 0, & Q^\alpha &= c G^\alpha, \end{aligned} \quad (2.10)$$

where G^α are the Gomis, Rodriguez-Gomez, Van Raamsdonk and Verlinde (GRVV) matrices [33, 35] defining a fuzzy two-sphere [34] at the matrix level N and $c = \sqrt{\frac{k\mu}{4\pi}}$. Let us note in passing that $c = 0$ gives a trivial solution in which both the fields Q^α and R^α vanish and is of no interest to us in what follows. Explicitly, G^α are given as [35]

¹Note that in the original model, i.e. in $2+1$ dimensions, the 't Hooft coupling is identified as $\lambda'_{tHooft} = \frac{N}{k}$ held fixed with $N, k \rightarrow \infty$ [33]. In the reduced model too, we may define $\tilde{\lambda}'_{tHooft} := \frac{N}{kV_2} = \frac{\lambda'_{tHooft}}{k}$ held fixed with $N, V_2 \rightarrow \infty$, while, in contrast, k can remain finite. In this case, scaling $\tilde{\lambda}'_{tHooft}$ to $\frac{1}{k}$ is the same as scaling λ'_{tHooft} to unity.

²In particular, let us note that pure CS action is indeed manifestly gauge invariant in $0+1$ - as opposed to the non-abelian CS action in $2+1$ -dimension, which is not. The latter gives rise to the level quantization of the CS coupling, i.e. $k \in \mathbb{Z}$. In fact, after the reduction of the CS terms to $0+1$ -dimensions but prior to introducing the 't Hooft parameter λ'_{tHooft} , the effective CS coupling is simply $\kappa := \frac{1}{4\pi} k V_2$ and is no longer an integral multiple of $\frac{1}{4\pi}$ due to the arbitrary volume V_2 of the two-dimensional compact space we have integrated over. This is consistent with the fact that CS term in $0+1$ -dimensions is gauge invariant and therefore its coupling is not level quantized. The latter also follows from the fact that $\pi_1(SU(N)) = 0$ and the general considerations on the gauge symmetry properties of $e^{iS_{CS}}$ which may be found, for instance, in [36, 37].

$$\begin{aligned}
(G^1)_{mn} &= \sqrt{m-1} \delta_{m,n}, \\
(G^2)_{mn} &= \sqrt{N-m} \delta_{m+1,n}, \\
(G_1^\dagger)_{mn} &= \sqrt{m-1} \delta_{m,n}, \\
(G_2^\dagger)_{mn} &= \sqrt{N-n} \delta_{n+1,m},
\end{aligned} \tag{2.11}$$

with $m, n = 1, \dots, N$, and they fulfill the relation

$$G^\alpha = G^\alpha G_\beta^\dagger G^\beta - G^\beta G_\beta^\dagger G^\alpha. \tag{2.12}$$

We may notice at this stage that, it is possible to work in the gauge with $A_0 = 0$ and $\hat{A}_0 = 0$. Evaluating the variations of S_{ABJM-R} with respect to A_0 and \hat{A}_0 , we find the Gauss law constraint is given by the two equations

$$\begin{aligned}
\frac{k}{2\pi} [X_1, X_2] + \dot{Q}^\alpha Q_\alpha^\dagger - Q^\alpha \dot{Q}_\alpha^\dagger + \dot{R}^\alpha R_\alpha^\dagger - R^\alpha \dot{R}_\alpha^\dagger &= 0, \\
-\frac{k}{2\pi} [\hat{X}_1, \hat{X}_2] - Q_\alpha^\dagger \dot{Q}^\alpha + \dot{Q}_\alpha^\dagger Q^\alpha - R_\alpha^\dagger \dot{R}^\alpha + \dot{R}_\alpha^\dagger R^\alpha &= 0.
\end{aligned} \tag{2.13}$$

It is also useful to note that the Hamiltonian takes the form

$$H = \text{Tr} \left(\frac{1}{N} |P_Q^\alpha|^2 + \frac{1}{N} \text{Tr} |P_R^\alpha|^2 + N |D_i Q^\alpha|^2 + N |D_i R^\alpha|^2 + NV \right), \tag{2.14}$$

where

$$P_Q^\alpha = \frac{\partial L}{\partial \dot{Q}^\alpha} = N \dot{Q}^{\alpha\dagger}, \quad P_R^\alpha = \frac{\partial L}{\partial \dot{R}^\alpha} = N \dot{R}^{\alpha\dagger}, \tag{2.15}$$

are the conjugate momenta associated to Q_α and R_α respectively. It is straightforward to see that the Hamiltonian for the CS part of the action vanishes identically as expected [37].

Let us consider the scaling transformation

$$(Q_\alpha, R_\alpha) \rightarrow (\rho^{-1/2} Q_\alpha, \rho^{-1/2} R_\alpha), \quad (X_i, \hat{X}_i) \rightarrow (\rho^{-1} X_i, \rho^{-1} \hat{X}_i), \quad t \rightarrow \rho t, \tag{2.16}$$

where ρ is an arbitrary positive constant. Under this scaling $(P_Q^\alpha, P_R^\alpha) \rightarrow (\rho^{-3/2} P_Q^\alpha, \rho^{-3/2} P_R^\alpha)$ and also that $V|_{\mu=0} \rightarrow \rho^{-3} V|_{\mu=0}$ indicating that the energy scales as $E \rightarrow \rho^{-3} E$. Since the Lyapunov exponent has the dimensions of inverse time, we see that it scales as

$$\lambda_L \propto E^{1/3}, \tag{2.17}$$

in the massless limit. In the ensuing sections, we will see that this scaling of the Lyapunov exponents with energy is essentially preserved after taking the mass deformations into account.

We are now in a position to propose ansatz configurations, through which we will be able to explore the emerging chaotic dynamics. We will consider two different ansatz configurations involving the GRVV matrices and satisfying the Gauss law constraints. Both of these ansatz configurations involve collective time-dependence which are introduced via real functions of time.

3 Ansatz I and the Effective action

The first matrix configuration we focus on is specified as follows:

$$\begin{aligned} X_i &= \alpha(t) \text{diag}((A_i)_1, (A_i)_2, \dots, (A_i)_N), \\ \hat{X}_i &= \beta(t) \text{diag}((B_i)_1, (B_i)_2, \dots, (B_i)_N), \\ Q_\alpha &= \phi_\alpha(t) G_\alpha, \quad R_\alpha = 0, \end{aligned} \quad (3.1)$$

where $(A_i)_m, (B_i)_m$ are constants and $i = 1, 2, m = 1, 2, \dots, N$ and $\alpha = 1, 2$. Thus, X_i and \hat{X}_i are taken as diagonal matrices. No sum over on the repeated index α is implied in the last line of (3.1). Here $\phi_\alpha(t), \alpha(t), \beta(t)$ are real functions of time and the Gauss law constraint given in the equation (2.13) is easily seen to be satisfied by this choice of the matrices.

Evaluating the equations of motion for $\alpha(t)$ and $\beta(t)$, we find that the emerging coupled equations have only one possible real solution and that is the trivial solution given simply as $\alpha(t) = \beta(t) = 0$. This result is proved in appendix (A). Henceforth, setting X_i and \hat{X}_i to zero and inserting last line of (3.1) in the action (2.8) and performing the traces over the GRV matrices at the level of $N \times N$ matrices, we obtain the reduced Lagrangian

$$L_N = N^2(N-1) \left(\frac{1}{2} \dot{\phi}_1^2 + \frac{1}{2} \dot{\phi}_2^2 - \frac{1}{2} \mu^2 (\phi_1^2 + \phi_2^2) - \frac{8\pi\mu}{k} \phi_1^2 \phi_2^2 - \frac{8\pi^2}{k^2} \phi_1^4 \phi_2^2 - \frac{8\pi^2}{k^2} \phi_1^2 \phi_2^4 \right). \quad (3.2)$$

The corresponding Hamiltonian is

$$\begin{aligned} H_N(\phi_1, \phi_2, p_{\phi_1}, p_{\phi_2}) &= \frac{p_{\phi_1}^2}{2N^2(N-1)} + \frac{p_{\phi_2}^2}{2N^2(N-1)} \\ &+ N^2(N-1) \left(\frac{1}{2} \mu^2 (\phi_1^2 + \phi_2^2) + \frac{8\pi\mu}{k} \phi_1^2 \phi_2^2 + \frac{8\pi^2}{k^2} \phi_1^4 \phi_2^2 + \frac{8\pi^2}{k^2} \phi_1^2 \phi_2^4 \right) \\ &=: \frac{p_{\phi_1}^2}{2N^2(N-1)} + \frac{p_{\phi_2}^2}{2N^2(N-1)} + V_N(\phi_1, \phi_2). \end{aligned} \quad (3.3)$$

where $V_N(\phi_1, \phi_2)$ introduced in the second line denotes the potential of this reduced system and defined by the relevant expression in the first line. For $k > 0$, we see that $V_N(\phi_1, \phi_2)$ is positive definite, while for $k < 0$ it is not, nevertheless the minimum of $V_N(\phi_1, \phi_2)$ is zero in both cases.

Let us note that, in the $\mu \rightarrow 0$ limit we have $H_N \rightarrow \rho^{-3} H_N$ under the scaling $(\phi_1, \phi_2) \rightarrow (\rho^{-1/2} \phi_1, \rho^{-1/2} \phi_2)$ and $t \rightarrow \rho t$, as can be readily expected in view of the discussion given at the end of the previous section.

To explore the dynamics of the model, we calculate the Hamiltonian's equations of mo-

tion. These take the form

$$\dot{\phi}_1 - \frac{p_{\phi_1}}{N^2(N-1)} = 0, \quad (3.4a)$$

$$\dot{\phi}_2 - \frac{p_{\phi_2}}{N^2(N-1)} = 0, \quad (3.4b)$$

$$\dot{p}_{\phi_1} + N^2(N-1) \left(\mu^2 \phi_1 + \frac{16\pi\mu}{k} \phi_1 \phi_2^2 + \frac{16\pi^2}{k^2} \phi_1 \phi_2^4 + \frac{32\pi^2}{k^2} \phi_1^3 \phi_2^2 \right) = 0, \quad (3.4c)$$

$$\dot{p}_{\phi_2} + N^2(N-1) \left(\mu^2 \phi_2 + \frac{16\pi\mu}{k} \phi_1^2 \phi_2 + \frac{16\pi^2}{k^2} \phi_1^4 \phi_2 + \frac{32\pi^2}{k^2} \phi_1^2 \phi_2^3 \right) = 0. \quad (3.4d)$$

In what follows, we will explore the dynamics emerging from the equations at $\mu = 1$ at several different matrix levels N and the CS coupling k .

In order to gain some immediate information on the system, it is useful to explore its fixed points and also investigate the stability around these points at the linear level. Details of this analysis are provided in appendix (B). In brief, for $k > 0$ the only fixed point of this Hamiltonian system is given as $(\phi_1, \phi_2, p_{\phi_1}, p_{\phi_2}) \equiv (0, 0, 0, 0)$ with a vanishing fixed point energy. Analysis in appendix (B) shows that this fixed point is of borderline type, meaning that the linear level analysis is inconclusive to identify it as either stable or unstable character and we do not attempt to perform a higher order analysis. For $k < 0$, we find that there are several fixed points, some of which are still of borderline type. Nevertheless, the set of fixed points given as $\left(\pm(\mp) \frac{\sqrt{-k}}{2\sqrt{3\pi}}, \pm \frac{\sqrt{-k}}{2\sqrt{3\pi}}, 0, 0 \right)$ are of unstable type. This latter fact may be taken as the first indication to expect the dynamics of H_N to be chaotic, since the latter is usually associated to the presence of unstable fixed points in the phase space [38–41].

3.1. Chaotic Dynamics and the Lyapunov Exponents

Lyapunov exponents are useful to determine the sensitivity of a system to given initial conditions. More precisely, they measure the exponential growth in perturbations and therefore give a reliable way to establish the presence of chaos in a dynamical system [38–41]. For a Hamiltonian system if we denote the perturbations in the phase space coordinates $\mathbf{g}(t) \equiv (g_1(t), g_2(t), \dots, g_{2N}(t))$ by $\delta\mathbf{g}(t)$, then we may conclude that the system is chaotic if, at large t , $\delta\mathbf{g}(t)$ deviates exponentially from its initial value at $t = t_0$: $\|\delta\mathbf{g}(t)\| = e^{\lambda(t-t_0)} \|\delta\mathbf{g}(t_0)\|$. Here λ are called the Lyapunov exponents and there are $2n$ of them for a phase space of dimension $2n$. Let us also note that this description is in parallel with the statement that even slightly different initial conditions give trajectories in the phase space, which are exponentially diverging from each other and hence lead to chaos. In a dynamical system, presence of at least one positive Lyapunov exponent is sufficient to conclude the presence of chaotic motion. In Hamiltonian systems, due to the symplectic structure of the phase space, Lyapunov exponents appear in λ_i and $-\lambda_i$ pairs and a pair of the Lyapunov exponents vanishes as there is no exponential growth in perturbations along the direction of the trajectory specified by the initial condition and the sum of all the Lyapunov exponents is zero as a consequence of Liouville's theorem. These facts are well-known and their details

may be found in many of the excellent books on chaos [38–41]. The phase space for the Hamiltonians H_N considered in this paper are all 4-dimensional. From the general considerations summarized above, it is clear that the emerging chaotic dynamics of these models are governed by the largest (and only) positive Lyapunov exponent at given values of the parameters k , μ and N .

In order to give a certain effectiveness to the random initial condition selection process, we adapt and use the simple approach we have developed in [14]. We briefly explain this next. Let us denote a generic set of initial conditions at $t = 0$ by $(\phi_1(0), \phi_2(0), p_{\phi_1}(0), p_{\phi_2}(0))$. First of all, we generate four random numbers and denote three of them as ω_i ($i = 1, 2, 3$) and define $\Omega_i = \frac{\omega_i}{\sqrt{\omega_i^2}}\sqrt{E}$, where E is the energy of the system. We denote the last random number as ω_4 . Clearly, we have $\sum_{i=1}^3 \Omega_i^2 = E$. With the help of this relation and the energy functional, i.e. Hamiltonian given in (3.3), initial conditions are picked randomly in the form

$$p_{\phi_1}(0) = \pm N\sqrt{(N-1)\Omega_1}, \quad p_{\phi_2}(0) = \pm N\sqrt{(N-1)\Omega_2}, \quad V_N(\phi_1(0), \phi_2(0)) = \Omega_3^2. \quad (3.5)$$

Finally, we select either $\phi_1(0)$ or $\phi_2(0)$ as ω_4 . Since V_N is invariant under $\phi_1 \leftrightarrow \phi_2$ exchange, which one of the two we select is immaterial. In our calculations, we take $\phi_2(0) = \omega_4$, then $\phi_1(0)$ is given by the solution of

$$V_N(\phi_1(0), \omega_4) - \Omega_3^2 = 0. \quad (3.6)$$

For some randomly picked values of ω_4 , (3.6) may not have a real solution. However, the code runs and randomly picks another ω_4 until a real solution for $\phi_1(0)$ is obtained.

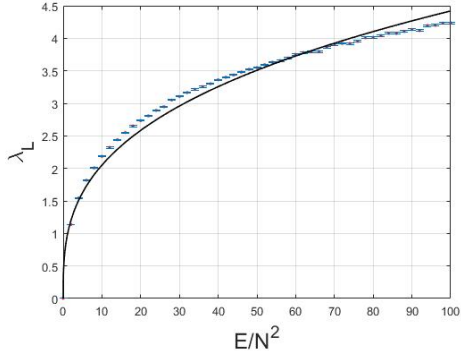
Similar to the analysis performed for the Yang-Mills matrix models with massive deformations presented in [9], we set up and run a MatLab code, which numerically solves the Hamilton's equations of motion given in (3.4) at different matrix levels. We run this code 40 times with randomly selected initial conditions at a given energy value E and matrix level N and calculate the mean of the time series for each and every Lyapunov exponent from all runs. In the simulation, we take a time step of 0.25 and run the code from time 0 to 1500. In particular, we focus on H_N for $N = 5, 10, 15, 20, 25$ at several different values of the energy.

3.2. Dependence of the Largest Lyapunov Exponent on Energy

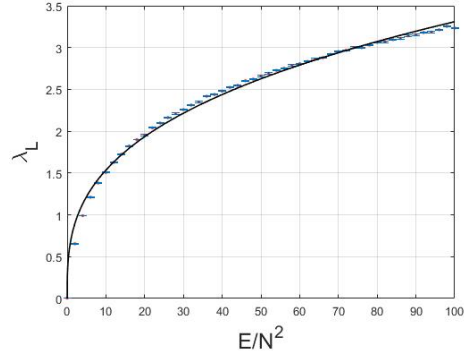
Since we are working in the 't Hooft limit, it is useful to consider the dependence of the largest Lyapunov exponent, λ_L on E/N^2 rather than on E , to capture the main features of the chaotic dynamics emerging from the family of Hamiltonian's H_N and subsequently relate it to the temperature of these systems via the use of virial and equipartition theorems.

Case i : $k \geq 1$

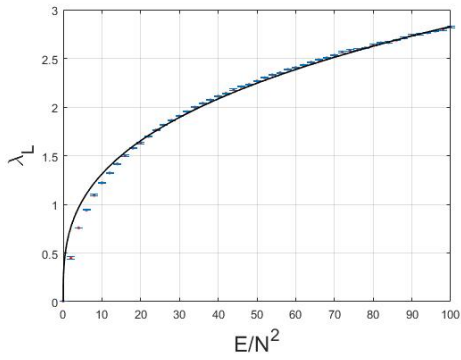
In this case, in order to capture the $\lambda_L \propto E^{1/3}$ dependence of the Lyapunov exponent anticipated by the scaling argument given in section 2, we find that it is sufficient to choose E/N^2 in the interval (0, 100). Lyapunov exponent data and the best fitting curves of the form $\lambda_L = \alpha_N(\frac{E}{N^2})^{1/3}$ are given in the figure (1) at $N = 5, 10, 15, 20, 25$.



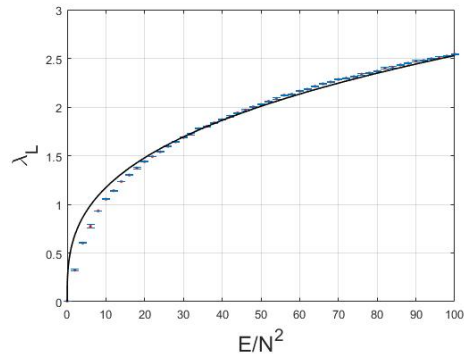
(a) $N = 5$



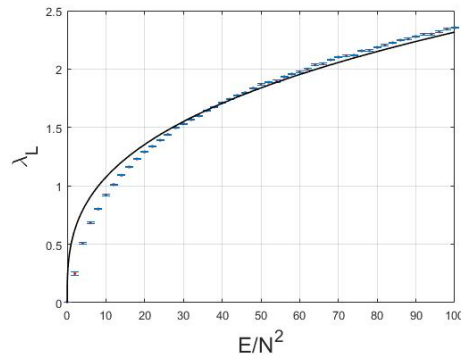
(b) $N = 10$



(c) $N = 15$



(d) $N = 20$

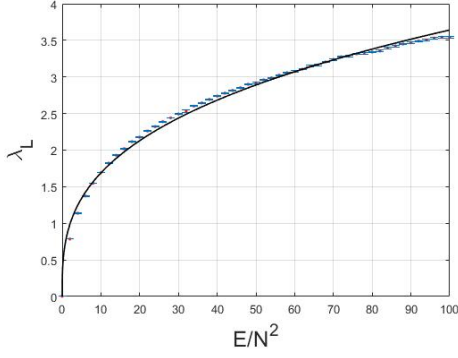


(e) $N = 25$

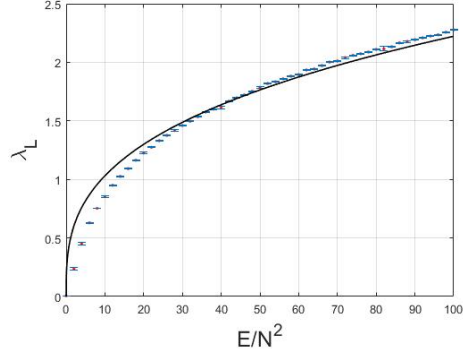
Figure 1: Largest Lyapunov exponent and the best fitting curves in the form $\lambda_L = \alpha_N (\frac{E}{N^2})^{1/3}$ at $k = 1$.

For $k = 2$, at sufficiently low matrix levels E/N^2 interval can still be taken as $(0, 100)$, while for $N > 20$, it turns out to be better to stretch it to a wider range, and in (2c), we take it to be $(0, 500)$. Lyapunov exponent data and the best fitting curves of the form $\lambda_L = \alpha_N (\frac{E}{N^2})^{1/3}$ are given in the figure (2).

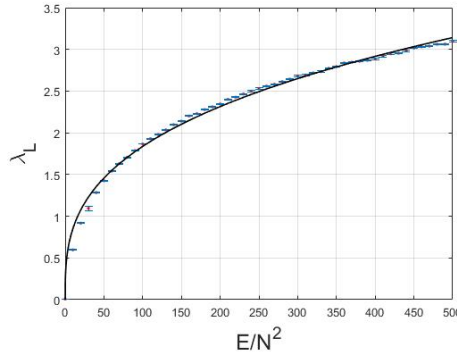
If we further increase the k value, we also need to inspect the dependence of λ_L to E/N^2



(a) $N = 5$



(b) $N = 15$



(c) $N = 25$

Figure 2: Largest Lyapunov exponent and the best fitting curves in the form $\lambda_L = \alpha_N \left(\frac{E}{N^2}\right)^{1/3}$ at $k = 2$.

in a sufficiently large range of the latter. For instance, in (3), we depict the Lyapunov data for $0 \leq E/N^2 \leq 500$, at the matrix level $N = 10$ and for $k = 5, 10$. At higher matrix levels or larger values k , it is necessary to further increase the range of E/N^2 in order to clearly observe the $E^{1/3}$ dependence of λ_L via the best fitting curves in the form $\lambda_L = \alpha_N \left(\frac{E}{N^2}\right)^{1/3}$. Coefficients α_N for the fitting curves in the figures (1), (2) and (3) are provided in the tables 1, 2 and 3 given in the next subsection.

Case ii : $k \leq -1$

In this case, the potential V_N is no longer positive definite and its minimum is negative as we have noted earlier. To compensate for this fact, we seek best fitting curves of the form $\lambda_L \propto \left(\frac{E}{N^2} - \gamma_N\right)^{1/3}$ to the Lyapunov data, where γ_N is determined by N , k and μ and proportional to the minimum value of \tilde{V}_N involving solely quartic terms from V_N . This specific form of the γ_N is indeed motivated by the virial and equipartition theorems as we will discuss it in the next subsection.

Both for $k = -1$ and $k = -2$, we find that $(0, 500)$ interval for E/N^2 is sufficiently well

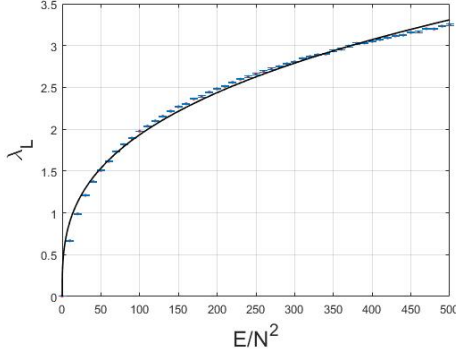
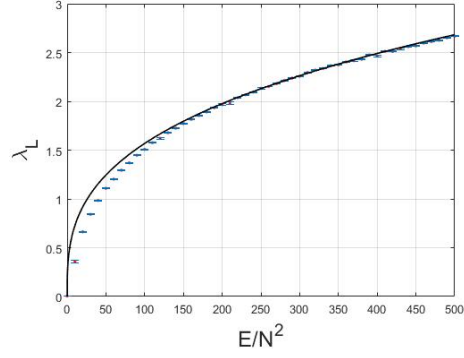
(a) $k = 5$ (b) $k = 10$

Figure 3: Largest Lyapunov exponent and the best fitting curves in the form $\lambda_L = \alpha_N \left(\frac{E}{N^2}\right)^{1/3}$ for $N = 10$ at $k = 5, 10$.

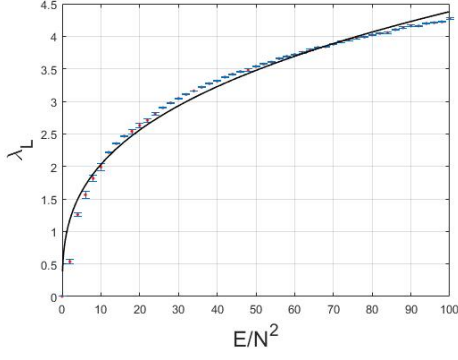
suites to capture the energy dependence of λ_L . This is corroborated by the best fitting curves of the form $\lambda_L = \alpha_N \left(\frac{E}{N^2} - \gamma_N\right)^{1/3}$ given in the figures (4) and (5). Coefficients α_N for the fitting curves in the figures (4), (5) and the respective values of γ_N are provided in the tables 4 and 5 in the next subsection.

3.3. Temperature dependence of the Lyapunov Exponent

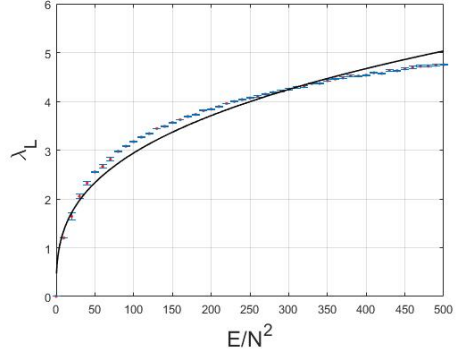
In [4], temperature dependence of the Largest Lyapunov exponent of the BFSS matrix model in the 't Hooft limit was determined using dimensional analysis to be of the form $\lambda_L \propto (\lambda_{tHooft} T)^{1/4}$ since λ_{tHooft} and the temperature are the only dimensionful parameters of the model. Let us note that this result is consistent with the fact that for the BFSS model the potential is purely quartic and the system has a scaling symmetry implying that $\lambda_L \propto E^{1/4}$ and hence $\lambda_L \propto T^{1/4}$ temperature dependence by evoking the equipartition theorem. In [14], we focused on a mass deformed Yang-Mills matrix theory, with the same matrix content as the bosonic part of the BFSS model and a similar analysis is considered where the effects of the mass deformations were taken into account in a simple way. For the present matrix model a similar approach can also be followed. We may expect that $\lambda_L \propto (\lambda_{tHooft} T)^\alpha$, where α is a constant that needs to be determined. As we noted in section 2, we may take $\lambda_{tHooft} = \frac{N}{V_2}$, where V_2 is the volume of the 2-dimensional space we have integrated over in going from $2 + 1$ to $0 + 1$ dimensions. From this definition of λ_{tHooft} , we see that it has the dimension of $[Length]^{-2}$, while we already know that each of λ_L and T have the dimension $[Length]^{-1}$. Putting these facts together, we have the following equation for α

$$[L]^{-1} = [L^{-2}L^{-1}]^\alpha = [L^{-3}]^\alpha, \quad (3.7)$$

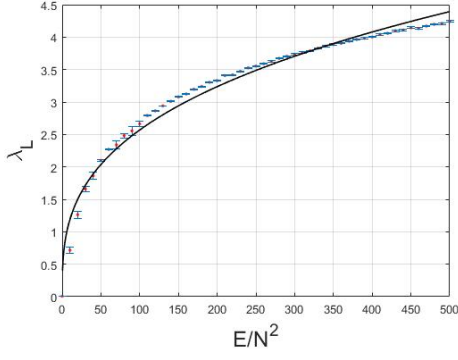
and therefore we find $\alpha = 1/3$. Thus, we may expect that $\lambda_L \propto (\lambda_{tHooft} T)^{1/3}$. In view of the equipartition theorem, this is consistent with the $\lambda_L \propto E^{1/3}$ based on the scaling symmetry as discussed in the previous section. Shortly, we will see the circumstances under which the



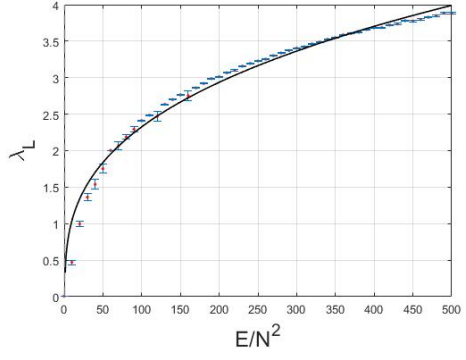
(a) $N = 5$



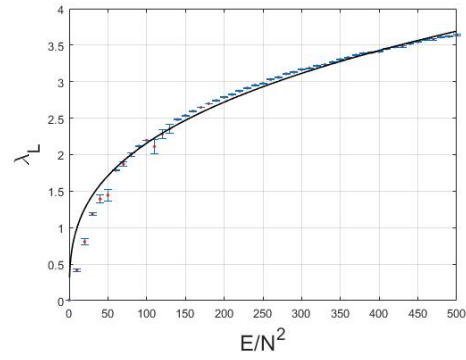
(b) $N = 10$



(c) $N = 15$



(d) $N = 20$



(e) $N = 25$

Figure 4: Largest Lyapunov exponent and the best fitting curves in the form $\lambda_L = \alpha_N(\frac{E}{N^2} - \gamma_N)^{1/3}$ at $k = -1$.

remaining dimensionful parameter, namely the mass, may effect the relation between the energy and temperature upon the application of the virial and the equipartition theorems. In order to prepare for the latter, let us first obtain the total number of independent degrees of freedom (d.o.f) of the ABJM matrix model described by the action (2.1). Here, we have both X_i and \hat{X}_i as $N \times N$ hermitian matrices with $i = 1, 2$. Each has N^2 real degrees of

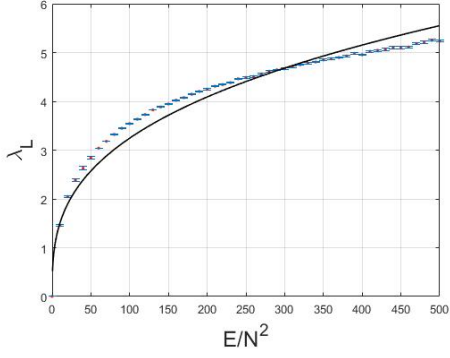
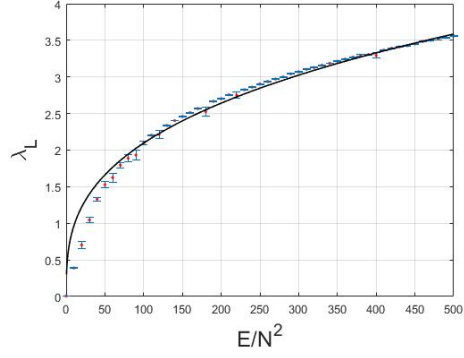
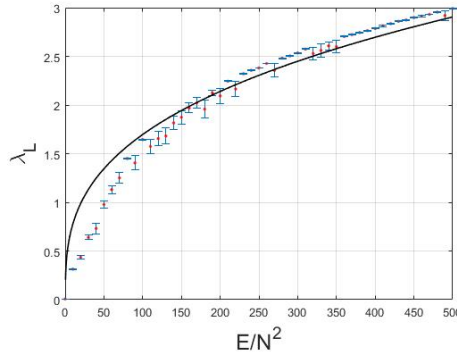
(a) $N = 5$ (b) $N = 15$ (c) $N = 25$

Figure 5: Largest Lyapunov exponent and the best fitting curves in the form $\lambda_L = \alpha_N \left(\frac{E}{N^2} - \gamma_N \right)^{1/3}$ at $k = -2$.

freedom and therefore these give $4N^2$ d.o.f. in total. We also have the fields Q^α and R^α with $\alpha = 1, 2$ as $N \times N$ complex matrices and each has $2N^2$ real d.o.f. leading to $8N^2$ real d.o.f. Therefore, the number of d.o.f. involved in the constituents of (2.8) is $4N^2 + 8N^2 = 12N^2$ before taking the global gauge symmetry and the constraints into account. Since the action is invariant under the R -symmetry group $SU(2) \times SU(2) \times U(1) \times U(1) \times Z_2$, each $SU(2)$ factor gives 3 and each $U(1)$ factor gives 1, and thus in total 8 real relations, while each of the equations in the Gauss law constraint (2.13) gives N^2 real relations among the unconstrained real degrees of freedom. Subtracting these from the latter, we find the independent d.o.f. count to be $12N^2 - 2N^2 - 8 = 10N^2 - 8$.

For the ansatz I in (3.1) there is a further reduction of the independent d.o.f. which comes about as follows. Since X_i and \hat{X}_i are null matrices due to vanishing of $\alpha(t)$ and $\beta(t)$ as the only admissible on-shell solution as argued in section 3 and demonstrated in appendix A, we need to subtract out a factor of $4N^2$. Additionally, due to the fact that $R_\alpha = 0$ in this ansatz, we need to subtract another factor of $4N^2$ d.o.f.. Finally, we also need to note that two equations of the Gauss law constraint reduce to the same equation upon integrating by

parts and taking the Hermitian conjugate of one or the other. Thus, the Gauss law constraint imposes only N^2 real relations in this case. These facts bring the total number of d.o.f. count to $10N^2 - 8 - 8N^2 + N^2 = 3N^2 - 8$. For large N , we may take $n_{d.o.f.} \approx 3N^2$.

Let us now apply the virial theorem to the Hamiltonian in (3.3). Since the potential $V_N(\phi_1, \phi_2)$ is not a homogeneous polynomial of its arguments, there is no exact proportionality relation linking the average kinetic and potential energies. Instead, we have

$$\begin{aligned} 2 \langle K \rangle &= 2 \langle V_N \rangle + 2N^2(N-1) \left(\frac{8\pi\mu}{k} \phi_1^2 \phi_2^2 + \frac{16\pi^2}{k^2} \phi_1^2 \phi_2^4 + \frac{16\pi^2}{k^2} \phi_1^4 \phi_2^2 \right) \\ &=: 2 \langle V_N \rangle + \tilde{V}_N(\phi_1, \phi_2), \end{aligned} \quad (3.8)$$

where the relevant expression in the first line provides the definition of $\tilde{V}_N(\phi_1, \phi_2)$ introduced on the second line. The latter is positive definite for $k > 0$ (assuming that $\mu > 0$ too, indeed we set $\mu = 1$) but not so for negative k . In fact, the minimum of $\tilde{V}_N(\phi_1, \phi_2)$ is given as :

$$\text{Min} \left(\tilde{V}_N(\phi_1, \phi_2) \right) = \begin{cases} 0 & \text{if both } k \text{ and } \mu \text{ have the same sign,} \\ N^2(N-1) \frac{k\mu^3}{27\pi} & \text{if } k \text{ and } \mu \text{ have the opposite sign.} \end{cases} \quad (3.9)$$

Applying the equipartition theorem to the kinetic energy yields

$$\langle K \rangle = \frac{1}{2}(3N^2 - 8)T \approx \frac{3}{2}N^2T, \quad (3.10)$$

where the approximation is valid at large N .

Case i: $k \geq 1$:

In this case, $\tilde{V}_N(\phi_1, \phi_2)$ is positive definite and therefore we have from (3.8) the inequality $\langle K \rangle \geq \langle V_N \rangle$. This and (3.10) together imply that $\langle E \rangle = \langle K \rangle + \langle V_N \rangle \leq n_{d.o.f.}T \approx 3N^2T$. We can express this inequality in the form

$$\frac{E}{N^2} \leq 3T, \quad (3.11)$$

where we have also dropped the brackets on energy for ease in notation.

Since, we expect that $\lambda_L \propto E^{1/3}$ due to the scaling properties of the model and also that $\lambda_L \propto T^{1/3}$ as implied by the pure dimensional analysis, albeit both holding exact only in the massless limit, we are, nevertheless, lead to examine the best fitting curves of the form

$$\lambda_L = \alpha_N \left(\frac{E}{N^2} \right)^{1/3}, \quad (3.12)$$

to profile the variation of the largest Lyapunov exponent as a function of E/N^2 . The fitting curves are plotted in the figure (1) for $k = 1$, $N = 5, 10, 15, 20, 25$, in the figure (2) for $k = 2$ at the matrix levels $N = 5, 15, 25$ and in the figure (3) for $k = 5, 10$ at the matrix level

Table 1: α_N and T_c values at $k = 1$.

	$N = 5$	$N = 10$	$N = 15$	$N = 20$	$n = 25$
α_N	0.9522	0.713	0.6092	0.5448	0.499
T_c	0.1022	0.0662	0.0523	0.0442	0.0388

Table 2: α_N and T_c values at $k = 2$.

	$N = 5$	$N = 15$	$N = 25$
α_N	0.7845	0.4788	0.3958
T_c	0.0764	0.0364	0.0274

Table 3: α_N and T_c values for $N = 10$ at $k = 1, 5, 10$.

	$k = 1$	$k = 5$	$k = 10$
α_N	0.6453	0.4168	0.3338
T_c	0.0570	0.0296	0.0212

$N = 10$. We observe that these fits represent the variation of the largest Lyapunov exponent with respect to E/N^2 remarkably well. Coefficients of α_N for the fitting curves are provided in the tables 1, 2 and 3.

We are now in a position to compare and relate our result to the MSS bound $\lambda_L \leq 2\pi T$ on the Largest Lyapunov exponent for quantum chaos [6]. This bound is conjectured to be satisfied in systems which are holographically dual to gravity, and it was shown in [7] that it is saturated for the Sachdev-Ye-Kitaev fermionic matrix model. In [4], chaotic dynamics of the BFSS matrix models was studied at the classical level, which provides an approximation to the quantum theory only in the high temperature limit, and it was shown that the largest Lyapunov exponent violates the MSS bound only at sufficiently low temperatures. Authors of [4] estimated the latter to be ≈ 0.015 . In [14], we studied a deformation of the bosonic sector of the BFSS via two mass terms and investigating the chaos in this model via reduced effective Lagrangians, we were able to put upper bounds on the critical temperature above which MSS inequality is satisfied, and below which it will eventually be violated. In [11, 12] a so-called Gaussian state approximation(GSA) is introduced to investigate the quantum chaotic dynamics of the BFSS and related Yang-Mills matrix models. Results obtained in [11, 12] demonstrate that the largest and all the other Lyapunov exponents tend to zero at a non-zero value of the temperature and therefore comply completely with the MSS conjecture at all temperatures. Nevertheless, it remains an open problem to show if and how the BFSS model saturates the MSS bound.

As we noted in the introduction, ABJM model has a gravity dual [33] via the AdS/CFT correspondence. Therefore, we may expect the MSS conjecture to hold for quantum chaotic

dynamics of the ABJM model too. In this article, we are investigating the dynamics of the mass deformed ABJM model only at the classical level so we should expect that the MSS bound be eventually violated at sufficiently low temperatures³.

Indeed using (3.11) and (3.12), we find that there is a critical temperature, which we may denote as T_c and given by solving the equation

$$\alpha_N(3T)^{1/3} = 2\pi T_c, \quad (3.13)$$

which yields

$$T_c = \sqrt{3} \left(\frac{\alpha_N}{2\pi} \right)^{3/2}. \quad (3.14)$$

From this result, we understand that for $T \geq T_c$ the present model complies with the MSS bound on λ_L , while $T \leq T_c$, there is a temperature at and below which MSS bound is not respected. Thus, we may say that T_c is an upper bound for the critical temperature at or below which MSS bound will eventually be violated by our model. The estimated T_c values at the matrix levels $N = 5, 10, 15, 20, 25$ are given in the tables 1 and 2 for $k = 1$, and $k = 2$, respectively and in the table 3 at $N = 10$ level for $k = 5, 10$. We observe from the values of T_c in these tables that with increasing matrix size their values tend to decrease, which is in agreement with the fact that 't Hooft limit is better emulated with increasing matrix size. From table 3, we also infer that T_c values tend to decrease with increasing values of k , i.e. the models with larger CS coupling tend to comply with the MSS conjecture within a wider range of the temperature.

Case ii: $k \leq -1$:

In this case, $\tilde{V}(\phi_1, \phi_2)_N$ is not positive definite as we have already noted, its minimum is negative and given by the expression in the second line of (3.9). Adding and subtracting $\left| \text{Min}(\tilde{V}_2) \right|$ to the (3.8), we may write

$$2\langle K \rangle = 2\langle V_N \rangle + \underbrace{\tilde{V}_N(\phi_1, \phi_2) + \left| \text{Min}(\tilde{V}_N) \right|}_{\geq 0} - \left| \text{Min}(\tilde{V}_N) \right|, \quad (3.15)$$

which implies that

$$\langle K \rangle \geq \langle V_N \rangle - \frac{1}{2} \left| \text{Min}(\tilde{V}_N) \right|. \quad (3.16)$$

We may therefore write

$$E = \underbrace{\langle K \rangle + \langle V_N \rangle - \frac{1}{2} \left| \text{Min}(\tilde{V}_N) \right|}_{\leq n_{d.o.f.} T} + \frac{1}{2} \left| \text{Min}(\tilde{V}_N) \right|. \quad (3.17)$$

³Let us note in passing that the presence of mass terms may keep the system away from saturating the MSS bound even if the full quantum dynamics could be studied. However, mass deformations lead to non-trivial vacuum solutions in the form of fuzzy sphere matrix configurations and provide us a good departure point to probe the chaotic dynamics as we do in the present paper.

Using $\langle K \rangle \approx \frac{3}{2}N^2T$ at large N , this leads to the inequality

$$\frac{E}{N^2} - \gamma_N \leq 3T, \quad \gamma_N := \frac{|Min(\tilde{V}_N)|}{2N^2}. \quad (3.18)$$

In view of this relation, we conjecture that the best fitting curves of the form

$$\lambda_N = \alpha_N \left(\frac{E}{N^2} - \gamma_N \right)^{1/3}. \quad (3.19)$$

These curves are given in the figure (4) for $N = 5, 10, 15, 20, 25$ at $k = -1$ and in the figure (5) for $N = 5, 15, 25$ at $k = -2$ and similar to the previous case they represent the variation of the largest Lyapunov exponent with respect to E/N^2 quite well. Coefficients of α_N for the fitting curves are provided in the tables 4 and 5. Let us note that, at larger values of N and $|k|$ for ($k < 0$) (for instance, $N = 25$ and $k = -2$) the mean square errors computed for λ_L at several values of E/N^2 are becoming larger as is observed from the errors bars provided in the figure 5c. This is essentially caused by the fact that some of the initial conditions randomly selected by our code to compute the mean value of the largest Lyapunov exponent coincide to a quasi-periodic orbit and therefore yield a vanishing Lyapunov exponent. This diminishes the mean λ_L value evaluated by averaging out the values obtained from the 40 initial conditions, and also leads to relatively larger mean square errors in λ_L . We suspect that the compatibility of the fitting curves of the form (3.19), for instance that of $N = 25$ and $k = -2$ given in figure 5c, will improve, should a more refined analysis of the Lyapunov data be performed. However, this is beyond the scope of our present focus in this paper.

Table 4: α_N, γ_N, T_c values at $k = -1$.

	$N = 5$	$N = 10$	$N = 15$	$N = 20$	$N = 25$
α_N	0.8120	0.6341	0.5539	0.5025	0.4971
γ_N	0.0944	0.2124	0.3300	0.4480	0.5660
T_c	0.0893	0.0697	0.0609	0.0553	0.0547

Table 5: α_N, γ_N, T_c values at $k = -2$.

	$N = 5$	$N = 15$	$N = 25$
α_N	0.6995	0.4522	0.3660
γ_N	0.1881	0.6600	1.1320
T_c	0.0769	0.0497	0.0403

By the same line of reasoning discussed in the previous case, using (3.18) and (3.19) we find that the critical temperature is given as

$$T_c = \sqrt{3} \left(\frac{\alpha_N}{2\pi} \right)^{3/2}, \quad (3.20)$$

and the numerical estimates using the α_N values of the fitting curves at several different matrix levels are listed in the tables 4 and 5 for $k = -1$ and $k = -2$, respectively.

Viewing the results of the cases *i)* and *ii)* together, we conclude that T_c values decrease with increasing N and/or $|k|$, i.e. the MSS bound is respected in a wider range of the temperature at matrix levels which better capture the 't Hooft limit and/or at larger values of the CS coupling.

4 Ansatz II

We would like to introduce another ansatz configuration with non-zero R_α and Q_α matrices and examine the ensuing dynamics. We consider the ansatz

$$\begin{aligned} Q_1 &= q(t)G_1, & R_1 &= r(t)G_1, \\ Q_2 &= q(t)G_2, & R_2 &= r(t)G_2, \end{aligned} \quad (4.1)$$

while we still take X_i and \hat{X}_i as arbitrary diagonal matrices as given in (3.1). This configuration satisfies the Gauss law constraints given in (2.13) as can easily be checked and the equations of motion for $\alpha(t)$ and $\beta(t)$ yields the only real solution as the trivial solution $\alpha(t) = \beta(t) = 0$ as shown in appendix A. Thus, in this case too, we set $X_i = 0 = \hat{X}_i$ in what follows.

Substituting the matrix configuration (4.1) into the action (2.8), and performing the trace over the GRVV matrices, we obtain the effective Lagrangian as

$$\begin{aligned} L(N) &= N^2(N-1) \left(\dot{q}^2 + \dot{r}^2 - \mu^2 q^2 - \mu^2 r^2 - \frac{8\pi\mu}{k} q^4 + \frac{8\pi\mu}{k} r^4 \right. \\ &\quad \left. + \frac{12\pi^2}{k^2} q^4 r^2 + \frac{12\pi^2}{k^2} q^2 r^4 - \frac{16\pi^2}{k^2} q^6 - \frac{16\pi^2}{k^2} r^6 \right). \end{aligned} \quad (4.2)$$

The corresponding Hamiltonian is

$$\begin{aligned} H(N) &= \frac{p_q^2}{4N^2(N-1)} + \frac{p_r^2}{4N^2(N-1)} + N^2(N-1) \left(\mu^2 q^2 + \mu^2 r^2 + \frac{8\pi\mu}{k} q^4 \right. \\ &\quad \left. - \frac{8\pi\mu}{k} r^4 - \frac{12\pi^2}{k^2} q^4 r^2 - \frac{12\pi^2}{k^2} q^2 r^4 + \frac{16\pi^2}{k^2} q^6 + \frac{16\pi^2}{k^2} r^6 \right) \\ &:= \frac{p_q^2}{4N^2(N-1)} + \frac{p_r^2}{4N^2(N-1)} + V_N(q, r), \end{aligned} \quad (4.3)$$

where $V_N(q, r)$ is the effective potential defined by the relevant terms in the first two lines of (4.3). A few remarks regarding the structure of $V_N(q, r)$ are now in order. Let us first note that this potential is not positive definite for either $k > 0$ or $k < 0$, while its minimum is at zero. Next, we easily see that $V_N(q, r)$ is symmetric under the exchange of q and r . For $k \leftrightarrow -k$ the two terms which are proportional to $\frac{1}{k}$ change sign, but this can be compensated by exchanging q and r . Thus, we conclude that the dynamics due to this potential is independent of the sign of k .

Hamilton's equations of motion are easily obtained and are given below:

$$\dot{q} - \frac{p_q}{N^2(N-1)} = 0, \quad (4.4a)$$

$$\dot{r} - \frac{p_r}{N^2(N-1)} = 0, \quad (4.4b)$$

$$\dot{p}_q + N^2(N-1) \left(2\mu^2 q + \frac{32\pi\mu}{k} q^3 - \frac{48\pi^2}{k^2} q^3 r^2 - \frac{24\pi^2}{k^2} q r^4 + \frac{96\pi^2}{k^2} q^5 \right) = 0, \quad (4.4c)$$

$$\dot{p}_r + N^2(N-1) \left(2\mu^2 r - \frac{32\pi\mu}{k} r^3 - \frac{24\pi^2}{k^2} q^4 r - \frac{48\pi^2}{k^2} q^2 r^3 + \frac{96\pi^2}{k^2} r^5 \right) = 0. \quad (4.4d)$$

To gain more insight about this Hamiltonian system, we explore its fixed points and their stability at the linear order. The details of this analysis are relegated to the appendix B. We find that for real values of μ either the set $(0, \pm \frac{\sqrt{k\mu}}{2\sqrt{3\pi}}, 0, 0)$ or the set $(\pm \frac{\sqrt{-k\mu}}{2\sqrt{3\pi}}, 0, 0, 0)$ give unstable fixed points for $k\mu > 0$ and $k\mu < 0$, respectively, and therefore the system is likely to have dynamical evolution which is chaotic. The remaining fixed points are of borderline type.

4.1. Dependence λ_L on Energy and Temperature

In order to obtain the profile of the mean largest Lyapunov exponent λ_L with respect to the variation of E/N^2 , we numerically solve the Hamilton's equations (4.4) and evaluate the mean of λ_L by averaging out the largest Lyapunov exponents over 40 runs of the code with randomly selected initial conditions. For this ansatz numerical aspects of the initial condition selection turns out to be somewhat more conveniently handled by setting $q(0) = 0$. Using three random numbers ω_i ($i = 1, 2, 3$) and writing $\Omega_i = \frac{\omega_i}{\sqrt{\omega_i^2}} \sqrt{E}$ as in the case of ansatz I, we generate the initial conditions in the form

$$p_\gamma(0) = \pm N \sqrt{(N-1)\Omega_1}, \quad p_\phi(0) = \pm N \sqrt{(N-1)\Omega_2}, \quad V_N(q(0) = 0, r(0)) = \Omega_3^2, \quad (4.5)$$

where the last equation in (4.5) takes the explicit form

$$N^2(N-1) \left(\mu^2 r(0)^2 - \frac{8\pi\mu}{k} r(0)^4 + \frac{16\pi^2}{k^2} r(0)^6 \right) - \Omega_3^2 = 0, \quad (4.6)$$

and its real roots are used to pick $r(t)$ at $t = 0$, i.e. the $r(0)$ value.

Applying the virial theorem, we find that

$$2\langle K \rangle = 2\langle V_N \rangle + \tilde{V}_N(q, r), \quad (4.7)$$

where

$$\tilde{V}_N(q, r) = N^2(N-1) \left(\frac{16\pi\mu}{k} q^4 - \frac{16\pi\mu}{k} r^4 - \frac{48\pi^2}{k^2} q^4 r^2 - \frac{48\pi^2}{k^2} q^2 r^4 + \frac{64\pi^2}{k^2} q^6 + \frac{64\pi^2}{k^2} r^6 \right). \quad (4.8)$$

Evaluating the minimum of $\tilde{V}_N(q, r)$, we find that it is given as

$$\text{Min}(\tilde{V}_N(q, r)) = -\frac{N^2(N-1)64|k\mu^3|}{135\sqrt{5}\pi}. \quad (4.9)$$

Following the same line of development and steps as in section 3.3., we have

$$\frac{E}{N^2} - \gamma_N \leq \frac{n_{d.o.f.}T}{N^2}, \quad \gamma_N := \left| \frac{\text{Min}(\tilde{V}_N(q, r))}{2N^2} \right|, \quad (4.10)$$

and therefore we are led to consider best fitting curves of the form

$$\lambda_L = \beta_N \left(\frac{E}{N^2} - \gamma_N \right)^{1/3} \quad (4.11)$$

to the λ_L versus E/N^2 data.

For all cases of interest it appears sufficient to use E/N^2 in the range (0, 100). For $k = \pm 1$, the data points and the fitting curves are depicted in the figure 6 for the matrix levels $N = 5, 10, 15, 20, 25$ and the β_N coefficients of the fits are given in the table 6.

Table 6: β_N , γ_N and T_c values at $k = \pm 1$.

	$N = 5$	$N = 10$	$N = 15$	$N = 20$	$N = 25$
β_N	0.6057	0.464	0.4006	0.3615	0.3346
γ_N	0.135	0.304	0.4725	0.64	0.81
T_c	0.0792	0.0531	0.0426	0.0365	0.0325

To profile the variation of λ_L at larger values of CS coupling, we first inspect the case $k = \pm 2$. Data points and fitting curves are given in the figure (7) and the corresponding β_N values are listed in table 7.

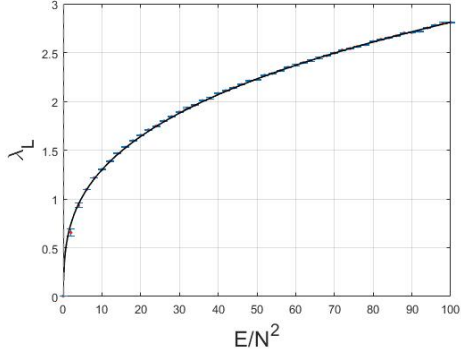
Table 7: β_N , γ_N and T_c values at $k = \pm 2$.

	$N = 5$	$N = 15$	$N = 20$	$N = 25$
β_N	0.4826	0.3164	0.2836	0.2622
γ_N	0.270	0.945	1.2822	1.62
T_c	0.0563	0.0299	0.0254	0.0226

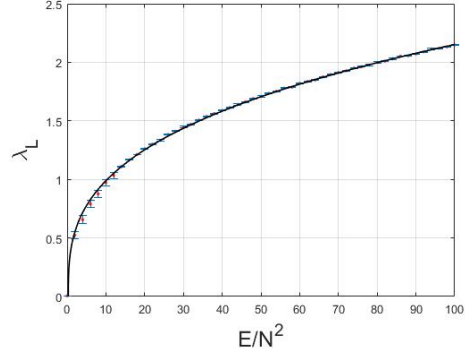
For $k = \pm 5, \pm 10$ the profile of λ_L and the fitting curves are provided in the figure 8 with β_N coefficients listed in the table 8.

From the plots provided in the figures 6, 7 and 8, we observe that the fitting curves represent the Lyapunov data remarkably well.

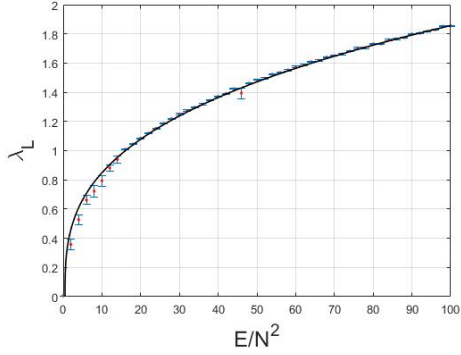
In order to obtain critical upper bound temperatures, T_c , using the coefficients β_N of the fitting curves, we need to count the independent degrees of freedom of the matrices given in



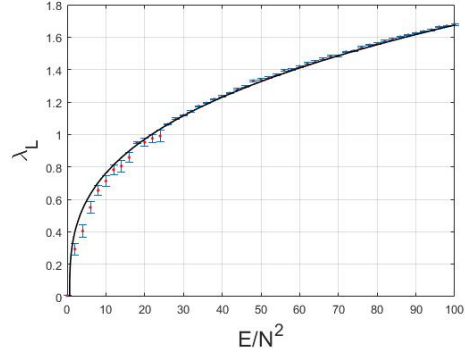
(a) $N = 5$



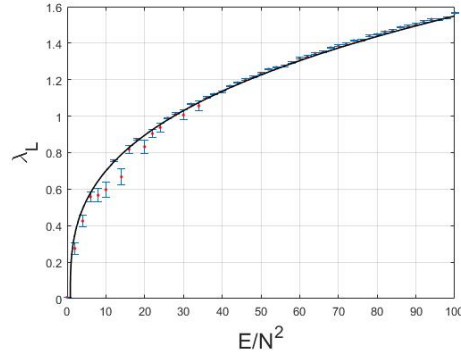
(b) $N = 10$



(c) $N = 10$



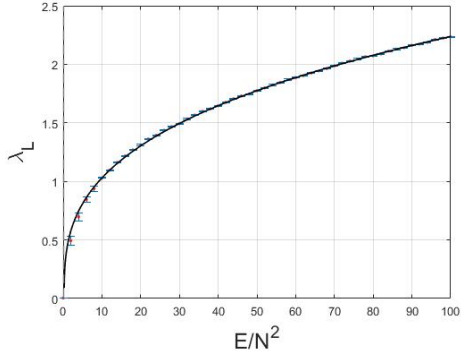
(d) $N = 20$



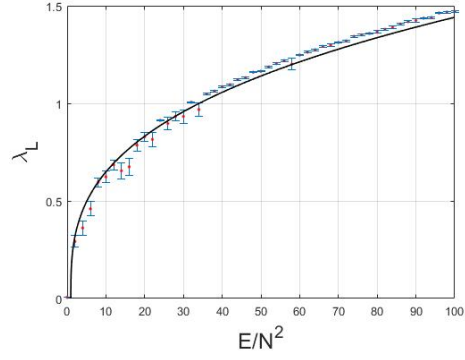
(e) $N = 25$

Figure 6: Largest Lyapunov exponent and the best fitting curves in the form $\lambda_L = \beta_N(\frac{E}{N^2} - \gamma_N)^{1/3}$ at $k = \pm 1$.

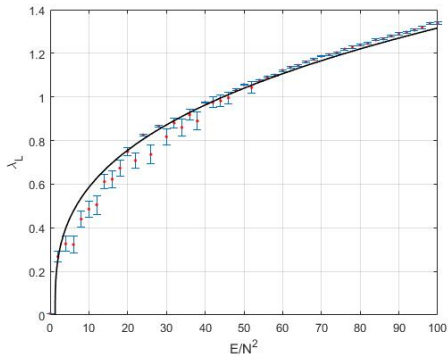
(4.1). In contrast to our first ansatz (3.1), in this case R_α matrices are no longer zero. Thus, we need to note that R_α ($\alpha = 1, 2$) contribute $4N^2$ degrees of freedom in total, while the two equations of the Gauss law constraint (2.13) imply the same condition upon integration by parts of one or the other equation. Thus, the Gauss law imposes only N^2 real constraints in this case too. We therefore have $n_{d.o.f.} = 7N^2 - 8$, which in the large N limit is given as



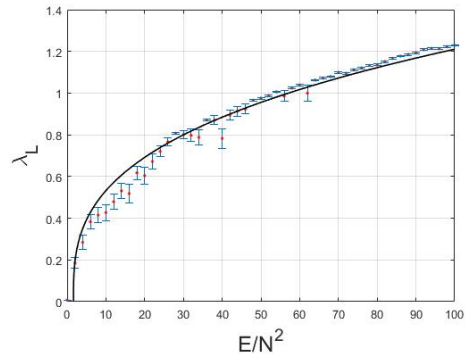
(a) $N = 5$



(b) $N = 15$

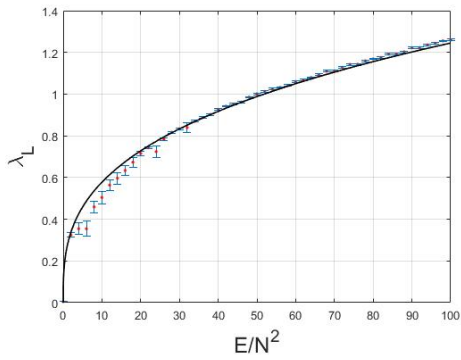


(c) $N = 20$

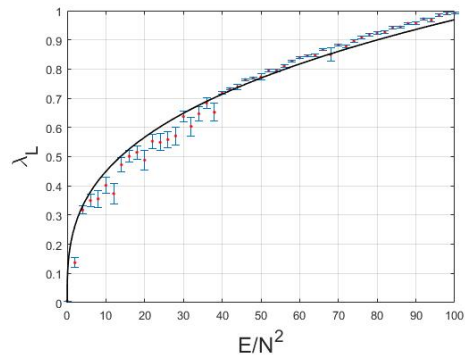


(d) $N = 25$

Figure 7: Largest Lyapunov exponent and the best fitting curves in the form $\lambda_L = \beta_N(\frac{E}{N^2} - \gamma_N)^{1/3}$ at $k = \pm 2$.



(a) $k = 5$



(b) $k = 10$

Figure 8: Largest Lyapunov exponent and the best fitting curves in the form $\lambda_L = \beta_N(\frac{E}{N^2} - \gamma_N)^{1/3}$ for $N = 10$ at $k = \pm 5, \pm 10$.

$n_{d.o.f.} \approx 7N^2$. Therefore, (4.10) immediately leads to the inequality

$$\frac{E}{N^2} - \gamma_N \leq 7T. \quad (4.12)$$

Table 8: β_N, γ_N values at $N = 10$ at $k = 1, 5, 10$.

	$k = 1$	$k = 5$	$k = 10$
β_N	0.4515	0.2716	0.2142
γ_N	0.304	1.5184	3.0369
T_c	0.051	0.0238	0.0167

We find that the critical temperature is obtained by solving

$$\beta_N(7T)^{1/3} = 2\pi T, \quad (4.13)$$

and this yields

$$T_c = \sqrt{7} \left(\frac{\beta_N}{2\pi} \right)^{3/2}. \quad (4.14)$$

Our estimates for the critical temperatures are given in tables 6, 7 and 8. Let us note classical chaotic dynamics of the family of effective Hamiltonians, H_N comply with the MSS bound for $T > T_c$, while they will eventually violate it at or below T_c values. Similar to the result obtained for ansatz I, we notice that with increasing matrix size and/or CS coupling values k , critical temperatures decrease. In particular, it is interesting to note that $T_c \approx 0.167$ for $N = 10$ and $k = \pm 10$, which is comparably close to ≈ 0.015 found in [4] for the BFSS model, although the two models are quite different in terms of the power law dependence of λ_L s on energy ($\propto E^{1/3}$ for the ABJM and $\propto E^{1/4}$ for the BFSS models).

5 Conclusions and Outlook

In this paper, we performed a detailed study of the chaotic dynamics of the mass deformed ABJM model. Working in the 't Hooft limit, and assuming that all the fields are spatially uniform and introducing ansatz configurations involving fuzzy spheres in the form of GRVV matrices with collective time dependence, we have obtained effective models and computed their Lyapunov exponents using numerical algorithms. Our results clearly indicate that these models possess chaotic dynamics. In particular, we directed our attention to the profile of the largest Lyapunov exponent and found that, depending on the form of the effective potential, either $\lambda_L \propto (E/N^2)^{1/3}$ or $\lambda_L \propto (E/N^2 - \gamma_N)^{1/3}$, where $\gamma_N(k, \mu)$ is a constant determined in terms of the Chern-Simons coupling k , the mass μ , and the matrix level N . They represent the result of the numerical findings considerably well as it is observed from the figures (1)-(8) and also further corroborated by the $\lambda_L \propto E^{1/3}$ power law dependence due to the scaling symmetry of the model in the massless limit. Upon the use of the virial and the equipartition theorems, we were able to examine the temperature dependence of the λ_L 's and derived critical upper bounds, T_c , on the temperature above which the MSS inequality, $\lambda_L \leq 2\pi T$, is respected and below which it will eventually be violated. Our numerical finding for these T_c values are presented in the tables given in sections 3 and 4, from which it is also observed that the T_c values display a decreasing trend with increasing matrix size, i.e. with the better

numerical emulation of the 't Hooft limit, as well as with the increasing values of the CS coupling k .

We strongly feel that the next step is to devise new methods to go beyond the classical analysis presented in the present paper, and explore the quantum dynamics of these models. The latter appears to be quite a formidable task. Nevertheless, inspired by the methods used in quantum chemistry in approaching many-body problems, recently a new real-time method⁴, which can be named as the Gaussian state approximation(GSA), is developed and thoroughly applied to the BFSS model [11, 12]. In its simplest form GSA aims at incorporating the quantum corrections by considering a larger but a truncated set of observable whose Heisenberg equations of motion are obtained via the use of a Gaussian density matrix. Application of this method to the BFSS model demonstrated that all the Lyapunov exponents tend to zero at a non-vanishing temperature implying that the quantum description of the BFSS model within the GSA approximation is fully compliant with the MSS inequality. However, given that it is still only an approximation of the full quantum dynamics, it falls short in providing an explicit saturation of the MSS bound by the Largest Lyapunov exponent, in contrast to the result for the SYK model obtained in [7] and expected for all models with holographic duals according to the MSS conjecture. We think that it will be extremely useful to attempt to apply the GSA to the ABJM model as well to the family of effective Hamiltonian's introduced in the present manuscript, not only to test the usefulness of GSA beyond the BFSS model but also to probe the quantum chaotic dynamics of the ABJM model. We hope to report on the possible developments along this direction elsewhere.

Acknowledgments

Authors acknowledge the support of TÜBİTAK under the project number 118F100.

References

- [1] Y. Sekino and L. Susskind, “Fast Scramblers,” JHEP **0810**, 065 (2008) doi:10.1088/1126-6708/2008/10/065 [arXiv:0808.2096 [hep-th]].
- [2] C. Asplund, D. Berenstein and D. Trancanelli, “Evidence for fast thermalization in the plane-wave matrix model,” Phys. Rev. Lett. **107**, 171602 (2011) doi:10.1103/PhysRevLett.107.171602 [arXiv:1104.5469 [hep-th]].
- [3] S. H. Shenker and D. Stanford, “Black holes and the butterfly effect,” JHEP **1403**, 067 (2014) doi:10.1007/JHEP03(2014)067 [arXiv:1306.0622 [hep-th]].
- [4] G. Gur-Ari, M. Hanada and S. H. Shenker, “Chaos in Classical D0-Brane Mechanics,” JHEP **1602**, 091 (2016) doi:10.1007/JHEP02(2016)091 [arXiv:1512.00019 [hep-th]].

⁴Most of the earlier investigations as well as some recent studies [42–46] have been aimed at investigating the phase structure of these models in the Euclidean time formulation using both analytical and Monte-Carlo methods.

- [5] D. Berenstein and D. Kawai, “Smallest matrix black hole model in the classical limit,” *Phys. Rev. D* **95**, no. 10, 106004 (2017) doi:10.1103/PhysRevD.95.106004 [arXiv:1608.08972 [hep-th]].
- [6] J. Maldacena, S. H. Shenker and D. Stanford, “A bound on chaos,” *JHEP* **1608**, 106 (2016) doi:10.1007/JHEP08(2016)106 [arXiv:1503.01409 [hep-th]].
- [7] J. Maldacena and D. Stanford, “Remarks on the Sachdev-Ye-Kitaev model,” *Phys. Rev. D* **94**, no.10, 106002 (2016) doi:10.1103/PhysRevD.94.106002 [arXiv:1604.07818 [hep-th]].
- [8] S. Aoki, M. Hanada and N. Iizuka, “Quantum Black Hole Formation in the BFSS Matrix Model,” *JHEP* **1507**, 029 (2015) doi:10.1007/JHEP07(2015)029 [arXiv:1503.05562 [hep-th]].
- [9] Y. Asano, D. Kawai and K. Yoshida, “Chaos in the BMN matrix model,” *JHEP* **1506**, 191 (2015) doi:10.1007/JHEP06(2015)191 [arXiv:1503.04594 [hep-th]].
- [10] E. Berkowitz, E. Rinaldi, M. Hanada, G. Ishiki, S. Shimasaki and P. Vranas, “Precision lattice test of the gauge/gravity duality at large- N ,” *Phys. Rev. D* **94**, no. 9, 094501 (2016) doi:10.1103/PhysRevD.94.094501 [arXiv:1606.04951 [hep-lat]].
- [11] P. Buividovich, M. Hanada and A. Schäfer, “Real-time dynamics of matrix quantum mechanics beyond the classical approximation,” *EPJ Web Conf.* **175**, 08006 (2018) doi:10.1051/epjconf/201817508006 [arXiv:1711.05556 [hep-th]].
- [12] P. V. Buividovich, M. Hanada and A. Schäfer, “Quantum chaos, thermalization, and entanglement generation in real-time simulations of the Banks-Fischler-Shenker-Susskind matrix model,” *Phys. Rev. D* **99**, no. 4, 046011 (2019) doi:10.1103/PhysRevD.99.046011 [arXiv:1810.03378 [hep-th]].
- [13] Ü. H. Coşkun, S. Kurkcuoglu, G. C. Toga and G. Unal, “Chaos from equivariant fields on fuzzy S^4 ,” *JHEP* **1812**, 015 (2018) doi:10.1007/JHEP12(2018)015 [arXiv:1806.10524 [hep-th]].
- [14] K. Başkan, S. Kürkçüoğlu, O. Oktay and C. Taşcı, “Chaos from Massive Deformations of Yang-Mills Matrix Models,” *JHEP* **10** (2020), 003 doi:10.1007/JHEP10(2020)003 [arXiv:1912.00932 [hep-th]].
- [15] S. G. Matinyan, G. K. Savvidy and N. G. Ter-Arutunian Savvidy, “Classical Yang-mills Mechanics. Nonlinear Color Oscillations,” *Sov. Phys. JETP* **53**, 421 (1981) [*Zh. Eksp. Teor. Fiz.* **80**, 830 (1981)].
- [16] G. K. Savvidy, “Yang-mills Classical Mechanics As A Kolmogorov K System,” *Phys. Lett.* **130B**, 303 (1983). doi:10.1016/0370-2693(83)91146-2

- [17] G. K. Savvidy, "Classical and Quantum Mechanics of Nonabelian Gauge Fields," Nucl. Phys. B **246**, 302 (1984). doi:10.1016/0550-3213(84)90298-0
- [18] T. Banks, W. Fischler, S. H. Shenker and L. Susskind, "M theory as a matrix model: A Conjecture," Phys. Rev. D **55**, 5112 (1997) doi:10.1103/PhysRevD.55.5112 [hep-th/9610043].
- [19] I. Y. Aref'eva, P. B. Medvedev, O. A. Rytchkov and I. V. Volovich, "Chaos in M(atrix) theory," Chaos Solitons Fractals **10**, 213 (1999) doi:10.1016/S0960-0779(98)00159-3 [hep-th/9710032].
- [20] D. E. Berenstein, J. M. Maldacena and H. S. Nastase, "Strings in flat space and pp waves from N=4 superYang-Mills," JHEP **0204**, 013 (2002) doi:10.1088/1126-6708/2002/04/013 [hep-th/0202021].
- [21] B. de Wit, J. Hoppe and H. Nicolai, "On the Quantum Mechanics of Supermembranes," Nucl. Phys. B **305**, 545 (1988) doi:10.1016/0550-3213(88)90116-2
- [22] N. Itzhaki, J. M. Maldacena, J. Sonnenschein and S. Yankielowicz, "Supergravity and the large N limit of theories with sixteen supercharges," Phys. Rev. D **58**, 046004 (1998) doi:10.1103/PhysRevD.58.046004 [arXiv:hep-th/9802042 [hep-th]].
- [23] K. Dasgupta, M. M. Sheikh-Jabbari and M. Van Raamsdonk, "Matrix perturbation theory for M theory on a PP wave," JHEP **0205**, 056 (2002) doi:10.1088/1126-6708/2002/05/056 [hep-th/0205185].
- [24] B. Ydri, "Review of M(atrix)-Theory, Type IIB Matrix Model and Matrix String Theory", arXiv:1708.00734 [hep-th].
- [25] B. Ydri, "Lectures on Matrix Field Theory," Lect. Notes Phys. **929**, pp.1 (2017) [arXiv:1603.00924 [hep-th]].
- [26] E. Kiritsis, *String theory in a nutshell*, Princeton University Press, 2007
- [27] K. N. Anagnostopoulos, M. Hanada, J. Nishimura and S. Takeuchi, Phys. Rev. Lett. **100**, 021601 (2008) doi:10.1103/PhysRevLett.100.021601 [arXiv:0707.4454 [hep-th]].
- [28] S. Catterall and T. Wiseman, Phys. Rev. D **78**, 041502 (2008) doi:10.1103/PhysRevD.78.041502 [arXiv:0803.4273 [hep-th]].
- [29] Aharony, O., Bergman, O., Jafferis, D. & Maldacena, J. " $\mathcal{N} = 6$ superconformal Chern-Simons-matter theories, M2-branes and their gravity duals," *Journal Of High Energy Physics*. **2008**, 091-091 (2008,10), <http://dx.doi.org/10.1088/1126-6708/2008/10/091>
- [30] D. N. Kabat and P. Pouliot, "A Comment on zero-brane quantum mechanics," Phys. Rev. Lett. **77** (1996), 1004-1007

- [31] V. Kares, “0-brane quantum chemistry,” Nucl. Phys. B **689** (2004), 53-75 doi:10.1016/j.nuclphysb.2004.04.008
- [32] K. Bařkan and S. K rk iođlu, “Chaos in the SU(2) Yang-Mills Chern-Simons matrix model,” Phys. Rev. D **104** (2021) no.6, 066006 doi:10.1103/PhysRevD.104.066006 [arXiv:2101.05649 [hep-th]].
- [33] Nastase, H. *Introduction to the ADS/CFT Correspondence*, Cambridge University Press, 2015.
- [34] A. P. Balachandran, S. Kurkcuoglu and S. Vaidya, *Lectures on Fuzzy and Fuzzy SUSY Physics*, Singapore, World Scientific, 2007, [hep-th/0511114].
- [35] Gomis, J., Rodr guez-G mez, D., Raamsdonk, M. & Verlinde, H. “A massive study of M2-brane proposals,” *Journal Of High Energy Physics*. **2008**, 113-113 (2008,9), <http://dx.doi.org/10.1088/1126-6708/2008/09/113>
- [36] A.P. Balachandran, G. Marmo, B.S. Skagerstam, A. Stern, *Classical Topology and Quantum States*, World Scientific, 1991.
- [37] G. V. Dunne, Aspects of Chern-Simons theory, in *Topological aspects of low dimensional systems Les Houches - Ecole d’Ete de Physique Theorique* p. 177–263, 1999, [arXiv:hep-th/9902115 [hep-th]].
- [38] E. Ott, *Chaos in Dynamical Systems*, Cambridge University Press, 2 ed., 2002.
- [39] R. Hilborn, *Chaos and Nonlinear Dynamics: An Introduction for Scientists and Engineers*, Oxford University Press, 1994.
- [40] S. L. Campbell and R. Haberman, *Introduction to differential equations with dynamical systems*, Princeton University Press, 2011.
- [41] I. Percival and D. Richards, *Introduction to Dynamics*, Cambridge University Press, 1983.
- [42] N. Kawahara, J. Nishimura and K. Yoshida, “Dynamical aspects of the plane-wave matrix model at finite temperature,” JHEP **06**, 052 (2006) doi:10.1088/1126-6708/2006/06/052 [arXiv:hep-th/0601170 [hep-th]].
- [43] N. Kawahara, J. Nishimura and S. Takeuchi, “Phase structure of matrix quantum mechanics at finite temperature,” JHEP **10**, 097 (2007) doi:10.1088/1126-6708/2007/10/097 [arXiv:0706.3517 [hep-th]].
- [44] R. Delgadillo-Blando, D. O’Connor and B. Ydri, “Geometry in Transition: A Model of Emergent Geometry,” Phys. Rev. Lett. **100**, 201601 (2008) doi:10.1103/PhysRevLett.100.201601 [arXiv:0712.3011 [hep-th]].

- [45] R. Delgadillo-Blando, D. O'Connor and B. Ydri, "Matrix Models, Gauge Theory and Emergent Geometry," JHEP **05**, 049 (2009) doi:10.1088/1126-6708/2009/05/049 [arXiv:0806.0558 [hep-th]].
- [46] Y. Asano, V. G. Filev, S. Kováčik and D. O'Connor, "The non-perturbative phase diagram of the BMN matrix model," JHEP **07**, 152 (2018) doi:10.1007/JHEP07(2018)152 [arXiv:1805.05314 [hep-th]].

A Equations of motion for $\alpha(t)$ and $\beta(t)$

1.1. Ansatz I

With the ansatz configuration given as

$$\begin{aligned} X_i &= \alpha(t) \text{diag}((A_i)_1, (A_i)_2, \dots, (A_i)_N) := \alpha(t) A_i, \\ \hat{X}_i &= \beta(t) \text{diag}((B_i)_1, (B_i)_2, \dots, (B_i)_N) := \beta(t) B_i, \\ Q_\alpha &= \phi_\alpha(t) G_\alpha, \quad R_\alpha = 0, \end{aligned} \tag{A.1}$$

and working in the $A_0 = 0$, $\hat{A}_0 = 0$ gauge, we immediately see that CS part of the action vanishes identically:

$$\begin{aligned} & - \frac{k}{4\pi} \text{Tr}(\epsilon^{ij} X_i \dot{X}_j) + \frac{k}{4\pi} \text{Tr}(\epsilon^{ij} \hat{X}_i \dot{\hat{X}}_j), \\ & = - \frac{k}{4\pi} \alpha \dot{\alpha} \text{Tr}[A_1, A_2] + \frac{k}{4\pi} \beta \dot{\beta} \text{Tr}[B_1, B_2], \\ & = 0. \end{aligned} \tag{A.2}$$

Next, we evaluate $\text{Tr} |D_i Q_1|^2 + \text{Tr} |D_i Q_2|^2$. We have,

$$\begin{aligned} (D_i Q_\alpha)_{ab} &= i(X_i Q_\alpha)_{ab} - i(Q_\alpha \hat{X}_i)_{ab}, \\ &= i(X_i)_{ac} (Q_\alpha)_{cb} - i(Q_\alpha)_{ac} (Q_\alpha)_{cb}, \end{aligned} \tag{A.3}$$

where the indices $a, b : 1, \dots, N$. Using (2.11), we obtain, for $\alpha = 1$

$$\begin{aligned} (D_i Q_1)_{ab} &= i(X_i Q_1)_{ab} - i(Q_1 \hat{X}_i)_{ab}, \\ &= i(X_i)_{ac} (\phi_1 G_1)_{cb} - i(\phi_1 G_1)_{ac} (\hat{X}_i)_{cb}, \\ &= i\alpha(t) \phi_1(t) (A_i)_{ac} \sqrt{c-1} \delta_{cb} - i\beta(t) \phi_1(t) \sqrt{a-1} \delta_{ac} (B_i)_{cb}, \\ &= i\alpha \phi_1 \sqrt{b-1} (A_i)_{ab} - i\beta \phi_1 \sqrt{a-1} (B_i)_{ab}, \\ &= i\phi_1 (\sqrt{b-1} X_i - \sqrt{a-1} \hat{X}_i)_{ab}, \\ &= i\phi_1 \sqrt{a-1} (X_i - \hat{X}_i)_{ab}, \end{aligned} \tag{A.4}$$

where the last line follows since X_i and \hat{X}_i are diagonal. The corresponding Hermitian conjugate is

$$(D_i Q_\alpha)_{ab}^\dagger = -i\phi_1 \sqrt{a-1} (X_i - \hat{X}_i)_{ba}. \tag{A.5}$$

These give

$$\begin{aligned}
\text{Tr} |D_i Q_1|^2 &= \text{Tr} (D_i Q_1)^\dagger (D_i Q_1) = (D_i Q_1)^\dagger_{ab} (D_i Q_1)_{ba}, \\
&= \phi_1^2 (a-1) \left((X_i^2)_{aa} + (\hat{X}_i^2)_{aa} - 2(X_i \hat{X}_i)_{aa} \right), \\
&= \phi_1^2 \sum_{\substack{a=1 \\ i=1,2}}^N (a-1) [\alpha^2 (A_a^i)^2 + \beta^2 (B_a^i)^2 - 2\alpha\beta A_a^i B_a^i], \\
&= \phi_1^2 \sum_{\substack{a=1 \\ i=1,2}}^N (a-1) (\alpha A_a^i - \beta B_a^i)^2.
\end{aligned} \tag{A.6}$$

Similarly, for $\alpha = 2$

$$(D_i Q_2)_{ab} = i(X_i)_{ac} \phi_2 (G_2)_{cb} - i(\phi_2 G_2)_{ac} (\hat{X}_i)_{cb}, \tag{A.7}$$

$$\begin{aligned}
&= i\phi_2 \sqrt{N-c} (X_i)_{ac} \delta_{c+1,b} - i\phi_2 \sqrt{N-a} \delta_{a+1,c} (\hat{X}_i)_{cb}, \\
&= i\phi_2 (\sqrt{N-b+1} (X_i)_{a,b-1} - \sqrt{N-a} (\hat{X}_i)_{a+1,b}), \\
&= i\phi_2 \sqrt{N-a} ((X_i)_{a,b-1} - (\hat{X}_i)_{a+1,b}),
\end{aligned} \tag{A.8}$$

with the Hermitian conjugate given as

$$(D_i Q_2)^\dagger_{ab} = -i\phi_2 \sqrt{N-a} ((X_i)_{b-1,a} - (\hat{X}_i)_{b,a+1}). \tag{A.9}$$

These give

$$\begin{aligned}
\text{Tr} |D_i Q_2|^2 &= \phi_2^2 (N-a) \left((X_i^2)_{a-1,a-1} + (\hat{X}_i^2)_{a+1,a+1} - (X_i)_{a,b-1} (\hat{X}_i)_{b,a+1} - (\hat{X}_i)_{a+1,b} (X_i)_{a,b-1} \right), \\
&= \phi_2^2 \sum_{\substack{a=1 \\ i=1,2}}^N (N-a) [\alpha^2 (A_{a-1}^i)^2 + \beta^2 (B_{a+1}^i)^2 - 2\alpha\beta A_a^i B_{a+1}^i].
\end{aligned} \tag{A.10}$$

We therefore have,

$$\text{Tr} |D_i Q_1|^2 + \text{Tr} |D_i Q_2|^2 = \alpha^2 S_1 + \beta^2 S_2 - 2\alpha\beta S_3, \tag{A.11}$$

where

$$\begin{aligned}
S_1 &= \phi_1^2 \sum_{\substack{a=1 \\ i=1,2}}^N (a-1) (A_a^i)^2 + \phi_2^2 \sum_{\substack{a=1 \\ i=1,2}}^N (N-a) (A_{a-1}^i)^2, \\
S_2 &= \phi_1^2 \sum_{\substack{a=1 \\ i=1,2}}^N (a-1) (B_a^i)^2 + \phi_2^2 \sum_{\substack{a=1 \\ i=1,2}}^{N-1} (N-a) (B_{a+1}^i)^2, \\
S_3 &= \phi_1^2 \sum_{\substack{a=1 \\ i=1,2}}^N (a-1) A_a^i B_a^i + \phi_2^2 \sum_{\substack{a=1 \\ i=1,2}}^{N-1} (N-a) A_a^i B_{a+1}^i.
\end{aligned} \tag{A.12}$$

Equation of motion for α and β take the form

$$\alpha S_1 - \beta S_3 = 0, \quad \beta S_2 - \alpha S_3 = 0, \quad (\text{A.13})$$

which yields

$$(S_1 S_2 - S_3^2) \alpha = 0. \quad (\text{A.14})$$

Since, $S_1 S_2 - S_3^2 \neq 0$, as one can see readily see by inspection (this is also verified using Mathematica at several different choices of N), therefore, the only solution to the equations of motion is the trivial solution:

$$\alpha(t) = 0, \quad \beta(t) = 0, \quad (\text{A.15})$$

as we intended to show.

1.2. Ansatz II

In this case, we immediately see by inspection from (4.4) and (A.12) that

$$\text{Tr} |D_i Q_1|^2 + \text{Tr} |D_i Q_2|^2 + |D_i R_1|^2 + \text{Tr} |D_i R_2|^2 = \alpha^2 T_1 + \beta^2 T_2 - 2\alpha\beta T_3, \quad (\text{A.16})$$

where

$$\begin{aligned} T_1 &= (q^2 + r^2) \left((N-1)(A_N^i)^2 + (N-2) \sum_{\substack{a=1 \\ i=1,2}}^{N-1} (A_a^i)^2 \right), \\ T_2 &= (q^2 + r^2) N \sum_{\substack{a=2 \\ i=1,2}}^N (B_a^i)^2, \\ T_3 &= (q^2 + r^2) \left(\sum_{\substack{a=1 \\ i=1,2}}^N (a-1) A_a^i B_a^i + \sum_{\substack{a=1 \\ i=1,2}}^N (N-a) A_a^i B_{a+1}^i \right). \end{aligned} \quad (\text{A.17})$$

with the equations of motion implying that

$$(T_1 T_2 - T_3^2) \alpha = 0. \quad (\text{A.18})$$

Since, $T_1 T_2 - T_3^2 \neq 0$, by inspection, the only solution to the equations of motion is, once again, the trivial solution $\alpha(t) = 0 = \beta(t)$.

B Fixed Points of the Reduced Lagrangians and their Stability

2.1. Ansatz I

Fixed points of a Hamiltonian system are defined as the stationary points of the phase space [14]. For the reduced dynamical system obtained using ansatz I, these points are given by the solutions of the equations

$$(\dot{\phi}_1, \dot{\phi}_2, \dot{p}_{\phi_1}, \dot{p}_{\phi_2}) = (0, 0, 0, 0). \quad (\text{B.1})$$

Combining (B.1) and the equations of motion given in (3.4) leads to four algebraic equations, two of which are trivially solved by $(p_{\phi_1}, p_{\phi_2}) \equiv (0, 0)$. The remaining two give us the coupled algebraic equations, which are expressed as

$$N^2(N-1) \left(\mu^2 \phi_1 + \frac{16\pi\mu}{k} \phi_1 \phi_2^2 + \frac{16\pi^2}{k^2} \phi_1 \phi_2^4 + \frac{32\pi^2}{k^2} \phi_1^3 \phi_2^2 \right) = 0, \quad (\text{B.2})$$

$$N^2(N-1) \left(\mu^2 \phi_2 + \frac{16\pi\mu}{k} \phi_1^2 \phi_2 + \frac{16\pi^2}{k^2} \phi_1^4 \phi_2 + \frac{32\pi^2}{k^2} \phi_1^2 \phi_2^3 \right) = 0. \quad (\text{B.3})$$

Fixed points may be determined by solving these equations.

Linear stability of the system may be inspected around a given fixed point, in order to determine whether it is a stable or unstable fixed point. A similar analysis was performed in [14] and we follow it in what follows. For simplicity, let us introduce the notation

$$(q_1, q_2, q_3, q_4) \equiv (\phi_1, \phi_2, p_{\phi_1}, p_{\phi_2}). \quad (\text{B.4})$$

From q_α and \dot{q}_α , we may form the Jacobian matrix

$$J \equiv [J]_{\alpha\beta} = \frac{\partial \dot{q}_\alpha}{\partial q_\beta}. \quad (\text{B.5})$$

The explicit form of J is given as

$$J = \begin{pmatrix} 0 & 0 & \frac{1}{N^2(N-1)} & 0 \\ 0 & 0 & 0 & \frac{1}{N^2(N-1)} \\ J_{31} & J_{32} & 0 & 0 \\ J_{41} & J_{42} & 0 & 0 \end{pmatrix}, \quad (\text{B.6})$$

where

$$\begin{aligned} J_{31} &= -N^2(N-1) \left(\mu^2 + \frac{96\pi}{k^2} \phi_1^2 \phi_2^2 + \frac{16\pi^2}{k^2} \phi_2^4 + \frac{16\pi\mu}{k^2} \phi_2^2 \right), \\ J_{32} &= -N^2(N-1) \left(\frac{64\pi^2}{k^2} \phi_1^3 \phi_2 + \frac{64\pi^2}{k^2} \phi_1 \phi_2^3 + \frac{32\pi\mu}{k} \phi_1 \phi_2 \right), \\ J_{41} &= -N^2(N-1) \left(\mu^2 + \frac{96\pi}{k^2} \phi_1^2 \phi_2^2 + \frac{16\pi^2}{k^2} \phi_1^4 + \frac{16\pi\mu}{k^2} \phi_1^2 \right), \\ J_{42} &= -N^2(N-1) \left(\frac{64\pi^2}{k^2} \phi_1^3 \phi_2 + \frac{64\pi^2}{k^2} \phi_1 \phi_2^3 + \frac{32\pi\mu}{k} \phi_1 \phi_2 \right). \end{aligned} \quad (\text{B.7})$$

Eigenvalues of J allow us to determine characteristic of a given fixed point. As it was summarized in [14], a fixed point is unstable if the Jacobian has at least one real positive eigenvalue. It may be that all the non-vanishing eigenvalues can be purely imaginary. In that case, the stability analysis is inconclusive and fixed point of borderline type and considerations beyond first order is necessary to decide on the characteristic of such a point.

At $\mu = 1$, for $k > 0$ the only real solution of the system given in (B.3) is the trivial solution $(\phi_1, \phi_2) \equiv (0, 0)$. Thus, the only fixed point of this Hamiltonian system is given as $(\phi_1, \phi_2, p_{\phi_1}, p_{\phi_2}) \equiv (0, 0, 0, 0)$ with vanishing energy, i.e. we have $E_F(0, 0, 0, 0) = 0$. We find that the eigenvalues of $J(0, 0, 0, 0)$ are given as $\{\pm i, \pm i\}$. Thus, this fixed point is of borderline type. We will not perform a higher order analysis for this fixed point.

For $k < 0$ and $\mu = 1$, the fixed points of the system are given as

$$(\phi_1, \phi_2, p_{\phi_1}, p_{\phi_2}) = \left\{ (0, 0, 0, 0), \left(\pm(\mp) \frac{\sqrt{-k}}{2\sqrt{\pi}}, \pm \frac{\sqrt{-k}}{2\sqrt{\pi}}, 0, 0 \right), \left(\pm(\mp) \frac{\sqrt{-k}}{2\sqrt{3\pi}}, \pm \frac{\sqrt{-k}}{2\sqrt{3\pi}}, 0, 0 \right) \right\}. \quad (\text{B.8})$$

Eigenvalues of the Jacobian at these fixed points are given as

$$\begin{aligned} J(0, 0, 0, 0) &\rightarrow \{ik, ik, -ik, -ik\}, \\ J\left(\pm(\mp) \frac{\sqrt{-k}}{2\sqrt{\pi}}, \pm \frac{\sqrt{-k}}{2\sqrt{\pi}}, 0, 0\right) &\rightarrow \{2ik, 2ik, -2ik, -2ik\}, \\ J\left(\pm(\mp) \frac{\sqrt{-k}}{2\sqrt{3\pi}}, \pm \frac{\sqrt{-k}}{2\sqrt{3\pi}}, 0, 0\right) &\rightarrow \left\{ -\frac{2k}{\sqrt{3}}, \frac{2k}{\sqrt{3}}, -\frac{2}{3}i\sqrt{5}k, \frac{2}{3}i\sqrt{5}k \right\}. \end{aligned} \quad (\text{B.9})$$

Thus the unstable fixed points are $\left(\pm(\mp) \frac{\sqrt{-k}}{2\sqrt{3\pi}}, \pm \frac{\sqrt{-k}}{2\sqrt{3\pi}}, 0, 0\right)$, since their Jacobian have a positive eigenvalue, while the remaining are of borderline type.

2.2. Ansatz II

Using the equations of motion given in (4.4), we find that the fixed points are determined by $(p_q, p_r) = (0, 0)$ and the solutions of the equations

$$\begin{aligned} \left(2\mu^2 q + \frac{32\pi\mu}{k} q^3 - \frac{48\pi^2}{k^2} q^3 r^2 - \frac{24\pi^2}{k^2} q r^4 + \frac{96\pi^2}{k^2} q^5 \right) &= 0, \\ \left(2\mu^2 r - \frac{32\pi\mu}{k} r^3 - \frac{48\pi^2}{k^2} q^2 r^3 - \frac{24\pi^2}{k^2} q^4 r + \frac{96\pi^2}{k^2} r^5 \right) &= 0. \end{aligned} \quad (\text{B.10})$$

We find that, for $k\mu > 0$ they are given as

$$(q, r, p_q, p_r) = \left\{ (0, \pm \frac{\sqrt{k\mu}}{2\sqrt{\pi}}, 0, 0), (0, \pm \frac{\sqrt{k\mu}}{2\sqrt{3\pi}}, 0, 0), (0, 0, 0, 0) \right\}, \quad (\text{B.11})$$

while for $k\mu < 0$ they are

$$(q, r, p_q, p_r) = \left\{ \left(\pm \frac{\sqrt{-k\mu}}{2\sqrt{\pi}}, 0, 0, 0 \right), \left(\pm \frac{\sqrt{-k\mu}}{2\sqrt{3\pi}}, 0, 0, 0 \right), (0, 0, 0, 0) \right\}. \quad (\text{B.12})$$

Jacobian matrix is again of the form given in (B.6), where now

$$\begin{aligned}
J_{31} &= -N^2(N-1) \left(\frac{480\pi^2}{k^2} q^4 - \frac{144\pi^2}{k^2} q^2 r^2 - \frac{24\pi^2}{k^2} r^4 + \frac{96\pi\mu}{k} q^2 + 2\mu^2 \right), \\
J_{32} &= -N^2(N-1) \left(\frac{96\pi^2}{k^2} q^3 r + \frac{96\pi^2}{k^2} q r^3 \right), \\
J_{41} &= -N^2(N-1) \left(\frac{96\pi^2}{k^2} q^3 r + \frac{96\pi^2}{k^2} q r^3 \right), \\
J_{42} &= -N^2(N-1) \left(\frac{480\pi^2}{k^2} r^4 - \frac{144\pi^2}{k^2} q^2 r^2 - \frac{24\pi^2}{k^2} q^4 - \frac{96\pi\mu}{k} r^2 + 2\mu^2 \right). \tag{B.13}
\end{aligned}$$

Eigenvalues of the Jacobian matrix at the fixed points are

$$J(0, 0, 0, 0) \rightarrow \left\{ -i\sqrt{2}\mu, -i\sqrt{2}\mu, i\sqrt{2}\mu, i\sqrt{2}\mu \right\}, \tag{B.14}$$

$$\begin{aligned}
J(0, \pm \frac{\sqrt{k\mu}}{2\sqrt{\pi}}, 0, 0) &\rightarrow \left\{ -\frac{i\mu}{\sqrt{2}}, \frac{i\mu}{\sqrt{2}}, -2\sqrt{2}i\mu, 2\sqrt{2}i\mu \right\}, \\
J(0, \pm \frac{\sqrt{k\mu}}{2\sqrt{3\pi}}, 0, 0) &\rightarrow \left\{ -2\sqrt{\frac{2}{3}}\mu, 2\sqrt{\frac{2}{3}}\mu, -i\sqrt{\frac{11}{6}}\mu, i\sqrt{\frac{11}{6}}\mu \right\}, \tag{B.15}
\end{aligned}$$

$$\begin{aligned}
J(\pm \frac{\sqrt{-k\mu}}{2\sqrt{\pi}}, 0, 0, 0) &\rightarrow \left\{ -\frac{i\mu}{\sqrt{2}}, \frac{i\mu}{\sqrt{2}}, -2\sqrt{2}i\mu, 2\sqrt{2}i\mu \right\}, \\
J(\pm \frac{\sqrt{-k\mu}}{2\sqrt{3\pi}}, 0, 0, 0) &\rightarrow \left\{ -2\sqrt{\frac{2}{3}}\mu, 2\sqrt{\frac{2}{3}}\mu, -i\sqrt{\frac{11}{6}}\mu, i\sqrt{\frac{11}{6}}\mu \right\}. \tag{B.16}
\end{aligned}$$

Therefore, for real values of μ , we have either the set $(0, \pm \frac{\sqrt{k\mu}}{2\sqrt{3\pi}}, 0, 0)$ or the set $(\pm \frac{\sqrt{-k\mu}}{2\sqrt{3\pi}}, 0, 0, 0)$ as unstable fixed points for $k\mu > 0$ and $k\mu < 0$, respectively, while the remaining fixed points are of borderline type. Let us finally observe that for purely imaginary values of μ (i.e. for tachyonic mass values), all these fixed points are of unstable type.